LBNL-39973
UC-413
Preprint

ERNEST ORLANDO LAWRENCE BERKELEY NATIONAL LABORATORY

Inclusive Dielectron Cross Sections in p+p and p+d Interactions at Beam Energies from 1.04 to 4.88 GeV

W.K. Wilson, S. Beedoe, R. Bossingham,
M. Bougteb, J. Carroll, W.G. Gong,
T. Hallman, L. Heilbronn, H.Z. Huang,
G. Igo, P. Kirk, G. Krebs, A. Letessier-Selvon,
L. Madansky, F. Manso, D. Magestro, H.S. Matis,
J. Miller, C. Naudet, R.J. Porter, M. Prunet,
G. Roche, L.S. Schroeder, P. Seidl, M. Toy,
Z.F. Wang, R.C. Welsh, and A. Yegneswaran

Nuclear Science Division

July 1997

Submitted to
Physical Review C

REFERENCE COPY
Does Not
Circulate
EP Bldg. 50 Library - Ref.
Lawrence Berkeley National Laboratory
Copy 1
LBNL-39973

DISCLAIMER

This document was prepared as an account of work sponsored by the United States Government. While this document is believed to contain correct information, neither the United States Government nor any agency thereof, nor the Regents of the University of California, nor any of their employees, makes any warranty, express or implied, or assumes any legal responsibility for the accuracy, completeness, or usefulness of any information, apparatus, product, or process disclosed, or represents that its use would not infringe privately owned rights. Reference herein to any specific commercial product, process, or service by its trade name, trademark, manufacturer, or otherwise, does not necessarily constitute or imply its endorsement, recommendation, or favoring by the United States Government or any agency thereof, or the Regents of the University of California. The views and opinions of authors expressed herein do not necessarily state or reflect those of the United States Government or any agency thereof or the Regents of the University of California.

LBNL-39973
UC-413

Inclusive Dielectron Cross Sections in p+p and p+d Interactions at Beam Energies from 1.04 to 4.8 GeV

W.K. Wilson,[a] S. Beedoe,[b] R. Bossingham,[c] M. Bougteb,[d] J. Carroll,[b] W.G. Gong,[c] T. Hallman,[e] L. Heilbronn,[c] H.Z. Huang,[c] G. Igo,[b] P. Kirk,[f] G. Krebs,[c] A. Letessier-Selvon,[c] L. Madansky,[e] F. Manso,[d] D. Magestro,[c] H.S. Matis,[c] J. Miller,[c] C. Naudet,[c] R.J. Porter,[c] M. Prunet,[d] G. Roche,[c,d] L.S. Schroeder,[c] P. Seidl,[b] M. Toy,[b] Z.F. Wang,[f] R.C. Welsh,[e] and A. Yegneswaran[c]

[a]Wayne State University, Detroit, Michigan 48201
[b]University of California at Los Angeles, California 90024
[c]Nuclear Science Division, Ernest Orlando Lawrence Berkeley National Laboratory, University of California, Berkeley, California 94720
[d]Université Blaise Pascal/IN2P3, 63177 Aubière Cedex, France
[e]The Johns Hopkins University, Baltimore, Maryland 21218
[f]Louisiana State University, Baton Rouge, Louisiana 70803

July 1997

This work was supported by the Director, Office of Energy Research, Office of High Energy and Nuclear Physics, Nuclear Physics Division, of the U.S. Department of Energy under Contract Nos. DE-AC03-76SF00098, DE-FG03-88ER40424, and DE-FG02-88ER40413.

Inclusive Dielectron Cross Sections in p+p and p+d Interactions at Beam Energies from 1.04 to 4.88 GeV

(The DLS Collaboration)

W.K. Wilson[a], S. Beedoe[b*], R. Bossingham[c], M. Bougteb[d],

J. Carroll[b†], W.G. Gong[c‡], T. Hallman[e§], L. Heilbronn[c],

H.Z. Huang[c#], G. Igo[b], P. Kirk[f], G. Krebs[c],

A. Letessier-Selvon[c**], L. Madansky[e], F. Manso[d],

D. Magestro[c††], H.S. Matis[c], J. Miller[c], C. Naudet[c‡‡],

R.J. Porter[c], M. Prunet[d], G. Roche[c,d], L.S. Schroeder[c], P. Seidl[b],

M. Toy[b], Z.F. Wang[f], R.C. Welsh[e§§], A. Yegneswaran[c##]

[a] *Wayne State University, Detroit, MI, CA 48201, USA*

[b] *University of California at Los Angeles, CA 90024, USA*

[c] *Lawrence Berkeley National Laboratory, University of California, Berkeley, CA 94720, USA*

[d] *Université Blaise Pascal/IN2P3, 63177 Aubière Cedex, France*

[e] *The Johns Hopkins University, Baltimore, MD 21218, USA*

[f] *Louisiana State University, Baton Rouge, LA 70803, USA*

Abstract

Measurements of dielectron production in p+p and p+d collisions with beam kinetic energies from 1.04 to 4.88 GeV are presented. The differential cross section is presented as a function of invariant pair mass, transverse momentum, and rapidity. The shapes of the mass spectra and their evolution with beam energy provide information about the relative importance of the various dielectron production mechanisms in this energy regime. The p+d to p+p ratio of the dielectron yield is also presented as a function of invariant pair mass, transverse momentum, and rapidity. The shapes of the transverse

momentum and rapidity spectra from the p+d and p+p systems are found to be similar to one another for each of the beam energies studied. The beam energy dependence of the integrated cross sections is also presented.

I. INTRODUCTION

Dielectrons (e^+,e^-) are penetrating probes of the hot and compressed nuclear matter produced in heavy-ion collisions because those produced in the interaction zone leave undisturbed by the surrounding nuclear medium [1–3]. The low mass continuum ($m \leq 1.0$ GeV/c^2) is particularly interesting since it provides information about pion and Δ dynamics in the excited nuclear medium at beam energies around 1 A·GeV [1–4]. However, attempts to extract information from measurements [5,6] of the low mass continuum in heavy-ion collisions have been hampered by the lack of cross section and form factor measurements for many of the processes which contribute to dielectron production. To address this problem, we have completed a systematic study of dielectron production in nucleon-nucleon interactions using the Dilepton Spectrometer (DLS) at the Lawrence Berkeley National Laboratory Bevatron. In this paper we present the first measured cross sections for dielectron production in p+p (pp) and p+d (pd) interactions at beam kinetic energies (T) ranging from 1 to 2 GeV. Since several of the fundamental dielectron production mechanisms are not yet well characterized, these measurements are interesting in their own right in addition to their importance in facilitating the interpretation of the heavy-ion studies. In particular, dielectron production in this beam energy range contains information about the electromagnetic form factor of the proton in a kinematical region which was not previously accessible [7].

We have previously published the differential cross sections[1] for T=4.88 GeV as well as

[1]The T=4.88 GeV data set reported here is the same data set that was reported as 4.9 in Ref. [8,10] and 4.84 GeV in Ref. [9]. The differences in the reported beam energies reflect successive refine-

the pd/pp yield ratios for each of the beam energies reported here [8–11]. In the interval since these publications we have made several changes in the data analysis, including refinements of the acceptance correction calculation, improvements in the tracking algorithm, and more accurate calibrations. Therefore, we will also show new versions of some of the previously published results in order to facilitate comparisons between different data sets within this paper. All of the differences between the current results and previously published data are either within the quoted systematic uncertainties or due to a new definition of the acceptance region. The change in the acceptance region will be discussed in detail below.

This paper is organized as follows. In the first section we briefly summarize the various categories of dielectron sources in this beam energy regime and review the results of other relevant measurements. The experimental conditions and data analysis are discussed in the second section. The resulting dielectron cross sections are presented in the third section, followed by the conclusion. The results of a pp elastic scattering study which checks some aspects of the data analysis are contained in the Appendix along with additional information on the acceptance correction.

A. Dielectron Production Mechanisms

A dielectron is an electron-positron pair which results from the decay of a massive virtual photon. For beam energies ranging from 1 to 5 GeV, the sources of dielectrons fall into three general categories: hadron decay, bremsstrahlung, and pion annihilation. We will briefly summarize these three categories and then discuss some of the unresolved theoretical issues about the dielectron mass distributions they produce. For an alternative explanation of dielectron production based upon a soft-parton-annihilation model, see Refs. [12].

Any hadron which has a decay branch leading to real photon production will also have a decay branch which produces a dielectron [13], albeit with a lower probability. Hadron

---

ments in the beam energy calculation.

decays can be divided into two sub-categories: two-body and Dalitz (multi-body). Only four particles are produced in our beam energy range which exhibit two-body decay to an electron-positron pair: the π°, ρ, ω, and ϕ mesons. However, the branching ratio of $\pi^\circ \rightarrow e^+e^-$ is so low that this channel can be ignored. There are several hadrons which undergo three-body Dalitz decays, including the Δ resonance [3,14,15] and the neutral mesons [16] π°, η, and ω. Unlike two-body decays which can produce recognizable peaks in the invariant mass spectra, Dalitz decays produce continuous mass distributions, making the isolation of their individual contributions a more difficult task. Estimation of the roles of specific Dalitz decay sources is somewhat easier in the pp system since one can compare the shape of the mass spectra above and below the absolute energy threshold for the formation of a source.

Dielectron production from bremsstrahlung processes forms the second category of sources. Early predictions indicated that pp bremsstrahlung would be negligible [1] and that pn bremsstrahlung would grow to dominate the dielectron yield as the beam energy increased from 1 to 5 GeV [17]. This view had to be re-examined when the pd/pp dielectron yield ratio at T=4.88 GeV was found to be only ≈ 2 [8,9]. The early predictions followed from considering only the "elastic" channel (two nucleons and a dielectron in the final state) and utilizing a non-relativistic approximation [18]. Subsequent studies [19,20] showed that this approximation was not valid in this energy regime. It was also found that at 4.88 GeV "inelastic" channels (final states involving one or more pions in addition to the nucleons and the dielectron) dominated the bremsstrahlung contribution to the dielectron yield. [21] These studies utilized the soft-photon approximation (no radiation from the interaction region) which requires accurate parameterizations of the elastic scattering cross sections [21,22]. Since the soft-photon approximation is not strictly applicable for dielectrons with masses above a few hundred MeV/c^2, one-boson exchange (OBE) studies have also been employed [23,24]. Unlike the soft-photon approximation, the OBE formalism allows radiation from the internal lines of the interaction diagram. Drawbacks of the OBE approach include the large number of diagrams which must be evaluated and ambiguities in adjusting

the parameters of the theory.

The third category of dielectron production mechanisms is pion annihilation. This can occur when oppositely charged pions annihilate in the hot pionic gas produced in a heavy-ion collision [1]. Dielectron production due to two pion annihilation is well described by the vector dominance model (VDM), producing a continuous mass spectrum with a prominent enhancement at the ρ mass. At T=4.88 GeV there is sufficient energy to produce up to twelve pions, but in simple p+nucleon collisions the magnitude of the pion annihilation source relative to the other dielectron sources is a subject of controversy [21,25,26].

B. Shapes of Dielectron Mass Spectra

In order to disentangle the contributions of the different dielectron sources it would be useful to know the shapes of the mass spectrum for each individual mechanism. In this section we will consider the uncertainties in the mass spectra shapes of processes mentioned above.

The shape of a dielectron mass spectrum produced by a vector meson decay is generally assumed to be a Breit-Wigner distribution centered on the meson mass. However, as Winckelmann et al. [26] recently pointed out, under some circumstances the shape of the mass spectrum produced by ρ meson decay may deviate strongly from this assumption due to phase space limitations. This can occur because ρ mesons produced through the decay of baryon resonances such as the N^*_{1520} and the N^*_{1680} have only limited phase space available for decay and thus the mass distribution peaks at lower values. For theoretical comparisons with the 4.88 GeV pp and pd dielectron data, this modification of the ρ mass distribution may play an important role [26] in filling in the mass region from 0.50 to 0.70 GeV/c^2. Some of the previous theoretical calculations which did not include this effect could not fully account for the observed cross section in this mass region for these systems [21].

The shape of the π° and η dielectron mass spectra created in hadron-hadron collisions are well explained using the VDM form factor (see Ref. [16] for a thorough review of electro-

magnetic decays of mesons). For the π° the Dalitz decay mode dominates and the two-body decay mode can be ignored. The ω Dalitz decay is believed to deviate strongly from VDM but to date only one measurement of its form factor has been performed. Although the shape of the ω Dalitz decay spectra is critical for understanding the hadron contributions to the low mass continuum at ultra-relativistic bombarding energies [27], for the energies considered here the ω cross section is small enough that the shape is not important [8].

There is a high degree of uncertainty in the shapes of the bremsstrahlung and Δ Dalitz decay mass spectra. They both depend on the coupling of the proton to the virtual photon through the proton electromagnetic form factor. The time-like form factor has been studied for dileptons with masses greater than twice the proton mass through the reaction $\mathrm{p} + \bar{\mathrm{p}} \rightarrow \mathrm{e}^- + \mathrm{e}^+$ and its inverse [28,29]. Lower mass dileptons cannot be studied using these reactions and are therefore said to reside in the "unphysical" region since their production would violate momentum and energy conservation. However, in bremsstrahlung and Δ Dalitz decay the proton goes off-shell and can therefore emit lower mass dielectrons, so the form factor in the unphysical region is a crucial element in predicting the shape of the mass spectra. One approach is to simply extend the VDM form factor into the unphysical region [21,30,31]. Several theoretical studies have concluded that this extension of the VDM form factor may produce an enhancement in the dielectron spectrum at the ρ-ω mass in nucleon-nucleon collisions at 2.1 GeV [31,32]. Thus, the data presented here may allow one to probe the proton form factor in a previously unexplored region.

The shape of the mass distribution produced by the two pion annihilation source depends on both VDM form factor and the momentum distribution of the pions [1]. The validity of VDM form factor for the pion is well established [16].

C. Other Measurements

Early studies of electron production detected only single electrons. Above T=10 GeV, single-electron measurements at low $p_\perp$ exhibited an e/π ratio of $\approx 10^{-3}$ [33], while below

T=1 GeV no electron signal was found down to an e/π ratio of $\approx 10^{-6}$ [34]. This suggested a threshold in electron production between 1 and 10 GeV. However, these single electron experiments could not provide any information on the mass or kinematics of dielectrons. Measurements performed with the DLS using p+Be (pBe) interactions from 1 to 5 GeV [35] confirmed the existence of a rapid rise in the dielectron cross section as a function of beam energy for pair masses greater than 200 MeV/c^2 (above the π^0 mass). However, three factors made it impossible to reach quantitative conclusions about the nature of the electron pair sources: the low statistics of the data, the combination of both pp and pn interactions in the same data sample, and the blurring of the particle thresholds due to the Fermi motion of the nucleons in the Be nucleus. The present data set removes all of these complications, making it easier to disentangle the continuum sources.

The experimental conditions and efficiencies are under much better control for the new pp and pd data sets than for the older pBe runs. In particular, we have found that the DLS exhibits a count rate dependent trigger inefficiency. This effect was not noted in the pBe data until a recent reanalysis of the T=4.9 GeV data was performed [36]. This reanalysis found an $\approx$80% loss of efficiency due to the high count rates in the 4.9 GeV pBe system which was not corrected for in the published cross sections. There is also angle dependent component of this inefficiency which will affect the shape of the mass spectra. We now know that all of the DLS data taken before 1990 show signs of this trigger inefficiency, but we lack sufficient diagnostic information to correct the published cross sections. For this reason, we suggest that data published from data runs before 1990 no longer be used for comparison with theory. We have corrected the pp and pd data sets for this inefficiency and will describe the procedure in the section on the normalization of the data.

Much of the interest in low-mass dilepton production in hadron-hadron collisions has focused on the possible existence of anomalous, *i.e.* previously unknown, sources. Above T=10 GeV, observations of dilepton production in excess of that predicted for conventional sources such as hadron decay have been reported in the past [37]. Recently, the HELIOS collaboration at CERN was able to explain the low-mass dilepton yield in 450 GeV/c pBe

interactions in terms of a hadron decay "cocktail" [27], placing an upper limit on any new source of electron pairs at 40% (90% confidence level). The two most important new elements of the cocktail were the use of the proper form factor in the ω Dalitz decay and a large increase in the cross section for η production. On the other hand, measurements of S+Au collisions at 200 A·GeV appear to show an excess of dielectrons above the predictions of the appropriate cocktail, reigniting the interest in the search for anomalous sources [38].

In the quest for uncovering new physics in anomalous sources, the expected sources are generally seen as background. However, from the standpoint of heavy-ion physics, detailed understanding of the conventional sources may provide unique information about the properties of excited, compressed nuclear matter. For example, the dielectron decay of the Δ provides information on resonance formation and dynamics within the fireball which is not available from the pionic decay channel since the pions interact strongly with the surrounding matter. In-medium modifications of vector mesons would create corresponding modifications in all the decays which obey the VDM. Of course, the ability to extract information from the dielectron continuum in heavy-ion reactions is ultimately dependent upon the ability to isolate the contributions of the various sources in nucleon-nucleon interactions.

II. EXPERIMENTAL DESCRIPTION

A. Apparatus

The DLS is a twin arm magnetic dipole spectrometer, and is described in Ref. [39]. Proton beams were provided by the Bevatron with T=1.04, 1.27, 1.61, 1.85, 2.09, and 4.88 GeV. For the data presented in this report, the solid target holder described in Ref. [39] was replaced by a cylindrical cryogenic vessel filled with liquid hydrogen, as described in [10]. The data was acquired in three periods of $\approx$1 month duration each, distributed over a period of three years, as summarized in Table I.

Electrons were distinguished from hadrons using two arrays of threshold Čerenkov gas

radiators coupled to phototubes [39]. In each arm, one bank of counters (front Čerenkovs) was placed upstream of the dipole field and a second bank (rear Čerenkovs) was placed downstream of the field.

The momenta of the electrons were extracted by reconstructing their paths through the magnetic field using space points from three drift chambers in each arm, one before and two behind the dipole fields. [39]. The invariant mass (m), transverse momentum ($p_\perp$), and laboratory rapidity (y) of the parent virtual photon were reconstructed from the momenta of the two electrons. The RMS mass resolution of the spectrometer is $\approx 10\%$ of the mass, independent of mass.

In order to check our overall normalization and our ability to correct for various efficiencies, we have studied the pp elastic scattering cross section. Our pp elastic measurement at 1.27 GeV is consistent with previous studies. We were also able to use the elastic scattering events to verify that our momentum scale was correctly calibrated. See Appendix A for details.

Data were taken with the target empty for some of the beam and target combinations in order to estimate the background due to electron pairs produced in interactions between the beam and the target assembly. Due to a target malfunction, the target could not be emptied for three of the systems studied in 1992. In addition, the number of pairs observed was ≤ 10 for six systems during the empty target running. These yields are too small to allow direct subtraction of the empty target background. Of the fourteen beam energy and target combinations[2], only five contained an adequate empty target pair sample for subtraction. Therefore, no subtraction of the empty target data has been performed for the data presented here. This does not adversely affect the quality of the data because the background is quite small. For the data set with the largest empty target sample, 4.88 GeV

[2]We have six beam energies and two targets, but the 4.88 GeV pd and pp were each measured twice, so there are a total of fourteen systems.

from 1990, the target full to target empty ratio was found to be approximately 10 for the pp data and 20 for the pd data. The ratios from the remaining systems with sufficient statistics for an estimate of the target in to target out ratio are consistent with these values.

B. Background subtraction

Data for like-sign (LS) pairs and opposite-sign (OS) pairs were acquired simultaneously. The "true" pairs, *i.e.* electron-positron pairs arising from a single electromagnetic vertex, form a subset of the OS sample. The remaining OS pairs make up the opposite-sign background (OSBK) which must be measured or reconstructed and subtracted from the from the OS sample. Background events are presumed to result from a combination of at least two instances of the following processes within the resolving time of the apparatus: γ conversion, π° Dalitz decay, Compton scattering, and hadron misidentification.

Over the years, the DLS collaboration has refined its techniques for estimating the OSBK as increases in dielectron statistics have allowed more detailed studies. Early on, the distribution of the electrons in the combinatoric background was found to be equivalent to that of the positrons within the limits of the available statistics. Under the assumption that the distributions of single electrons and single positrons are identical, the OSBK should be identical to the LS sample and the true pairs can be obtained by simply subtracting the LS sample from the total OS sample. This technique was employed in the analysis of the early, lower statistics DLS data [5,6,35,40,41]. However, for the much higher statistics data samples reported here, a momentum dependent excess of electrons over positrons was found in the LS sample. One reason for this asymmetry could be Compton scattering of photons which generates electrons exclusively.

In circumstances where the electrons and positrons have different source properties, it is possible to determine the shape of the combinatoric OSBK via mixing of electrons and positrons from LS pairs across different events. The size of the OSBK using this algorithm is compared in Fig. 1 to the OS and true pair samples for the pd system at 1.04 and 4.88

GeV. An advantage of this approach is that a very high degree of statistical precision can be reached in the construction of the OSBK. However, systematic errors may be introduced by this method since the OSBK derived from the event mixing technique may fail to reproduce subtle correlations in the actual OS background. For example, the true background must not violate conservation of energy on an event by event basis, while the event mixed background is not similarly constrained. We could not evaluate the accuracy of the event mixing technique directly since we had no independent measurement of the OSBK. However, the LS sample is also composed of purely random coincidences, and it was directly measured. Any systematic bias which affects the generated OSBK should become apparent if one compares the measured LS sample to a LS sample generated by event mixing. In order to evaluate such biases, we compare in Fig. 2 an event mixed estimation of the LS sample with the actual measured LS sample for the 1.04 and 4.88 GeV pd data. The estimates of the systematic uncertainty in the shapes of the differential cross sections shown in the following figures were derived in part from comparisons such as these.

C. Normalization

Several cuts were used to minimize the OSBK, therefore the overall normalization must be corrected in the final spectra. For example, hadrons may be misidentified as electrons if they scintillate in the Čerenkov gas. The scintillation of hadrons produces a relatively weak signal compared to the Čerenkov radiation of electrons, so hadron misidentification was minimized by placing a requirement on the minimum pulse height, equivalent to two tenths the average electron signal. Since both members of a dielectron generated by a photon conversion will often go into a single front Čerenkov counter due the pair's small opening angle, it will produce a Čerenkov pulse height which is twice the size of that produced by a single electron. A limit was placed on the maximum Čerenkov pulse height to suppress this background. These cuts result in a total Čerenkov efficiency for detecting a dielectron (signals in all four counters) to 93.8%. Any remaining hadron contamination is removed in

the background subtraction.

The rear Čerenkov counter in each arm are divided into ten modules above and ten modules below the spectrometer midplane. The top modules were found to be less efficient than the bottom modules, leading to a loss of 9.3% to 16.7% of pairs, depending on the data set. The cause of this inefficiency was not determined.

The Čerenkov counters reduced the hadron contamination sufficiently so that it was not necessary to use time of flight cuts to further distinguish hadrons from electrons. However, cuts were placed on the time differences between tracks in the two arms of the spectrometer to minimize random coincidences between unrelated events. These cuts resulted in no significant loss in pair efficiency for true pairs.

Events which contained more than two electrons were found to yield equal numbers of LS and OS pairs, implying that all of the OS pairs were due to combinatoric background. Rejecting these events from the analysis resulted in a further 2.1% loss in pair efficiency.

The tracking efficiency for dielectrons due to drift chamber wire plane and algorithmic efficiencies was evaluated for each data set and varied from 47% to 66%. The low end of the efficiency range was caused by a hardware problem which affected the drift chambers for some of the data sets. In some data sets, we also found that there was a reduction in the tracking efficiency at small angles with respect to the beam. We have corrected for this effect by applying a minimum angle requirement to eliminate the data which was most strongly affected and by applying an angle dependent efficiency correction to the remaining pairs. The same minimum angle cut was applied to all of the data in order to simplify comparisons between data sets. This cut has the effect of increasing the minimum pair opening angle which the DLS can measure, decreasing the DLS acceptance for low mass pairs (below 0.2 GeV/c^2). Therefore, the definition of the DLS acceptance region (discussed below) has been recalculated for the current data set. Due to the change in the angular acceptance of the spectrometer which results from the minimum angle cut, we are not able to present data for masses below 0.10 GeV/c^2. A cut placed on the χ^2 of the reconstructed tracks resulted in a loss of 4.5% of the dielectron pairs.

The time averaged detector count rates were monitored to insure that they did not exceeded the capacity of the trigger electronics. For about half of the beam/target combinations we also acquired a small subset of the data at lower count rates than those in our standard running conditions. Comparing data acquired at low detector count rates to that taken at normal count rates allowed us to check for any rate dependent trigger efficiency. When we analyzed the results we did find a significant rate dependence trigger inefficiency, especially in the data acquired in 1990 and 1991. Improvements in the triggering electronics helped to minimize this problem in the 1992 data. The inefficiency was believed to be due to high frequency structures in the beam provided by the Bevatron. Although the count rates were below the limit of the trigger electronics when averaged over long time scales, we found that they were exceeding the limit when evaluated on the shorter time scales relevant to the trigger electronics, on the order of hundreds of nanoseconds. This was confirmed using a delayed coincidence rate monitor during the 1992 runs which was sensitive to the high frequency structure in the Bevatron spill. In order to correct for this inefficiency, we evaluated its count rate dependence for data sets taken at both normal and low count rates, and we assumed the same dependency for data sets taken only at the normal rates. The 1990 data sets suffered efficiency losses of up to 56%, while some 1992 data sets exhibited no efficiency loss. Note that the cross sections for the 1990 data presented in previous DLS publications [8,10] were also corrected for this inefficiency.

The data sets taken at low count rates contained low statistics, so the rate dependent correction dominated the systematic uncertainty in the overall normalization. This statistical uncertainty in the rate dependent trigger efficiency generated the overall normalization uncertainties displayed in Table II. Since they do not affect the shape of the spectra, these uncertainties are not displayed in the plots of differential cross sections presented in this paper. However, they must be taken into consideration when comparing with theoretical predictions. Overall systematic normalization uncertainties for the pd/pp ratios are also presented in Table II.

D. Acceptance Correction

The techniques employed by the DLS group to correct for the spectrometer's geometrical acceptance have been refined as the size of our pair sample has increased. The philosophy behind the acceptance correction is described in detail in Appendix B.

The acceptance region is the volume in m-$p_\perp$-y space within which our simulations indicate that it is possible for us to reliably report the cross section. For the current data set, we have enlarged the definition of the acceptance region slightly in some areas, restricted it in others due to the tracking inefficiency at small angles discussed earlier, and refined our definition of the edges in general. These changes primarily affect the mass spectra only in the region below 0.2 GeV/c^2. This change in the definition of the acceptance region requires that all those who wish to compare theory with this DLS data obtain a copy of version 4 of the m-$p_\perp$-y filter code, available from the authors upon request. In addition to filtering the theory through the acceptance region, the theory must also be smeared according to the DLS resolution before projecting out m, $p_\perp$, or y spectra for comparison with the data. This smearing is now included as an option in the DLS filter code. The DLS acceptance strongly affects the shapes of the mass spectra below 0.20 GeV/c^2 and the entire range of the transverse momentum spectra and rapidity spectra. The extreme edges of the DLS acceptance for this data set are $0.1 \leq m \leq 1.25$ GeV/c^2, $0.0 \leq p_\perp \leq 1.2$ GeV/c, and $0.5 \leq y \leq 1.7$.

An example of the effect of the acceptance correction is shown in Fig. 3 for the 4.88 GeV pd mass spectra. The uncorrected spectra is multiplied by a factor of 100 in order to facilitate the comparison. Note that the acceptance correction is largest for the lowest masses. This is because the spectrometer's acceptance is more restricted for low mass pairs due to their smaller dielectron opening angles.

III. DIELECTRON CROSS SECTIONS

A. Mass Spectra

Invariant mass spectra for the pd and pp systems are denoted by filled and unfilled circles respectively in Fig. 4 for the six beam energies. The kinematical upper limit on the pair mass produced in the pp system is indicated by a dotted line in the lower portion of each panel except for the 4.88 GeV data set where the limit is off scale. Note that the momentum resolution discussed earlier will allow pairs to be reconstructed above the kinematical limit in the pp system. The error bars on each data point indicate only the statistical uncertainties. The brackets above and below the low mass data points indicate our estimate of the systematic uncertainties in the shape of the spectra in this region added linearly with the statistical uncertainties. The overall normalization uncertainties are not shown in the figure since they do not affect the shape of the distributions. The standard bin width is 50 MeV/c^2, however, some of the points have been rebinned to take the sparse statistics into account. The bins with enlarged widths are indicated by horizontal bars. All of the differential cross section plots which follow are displayed in the same format.

The shape of these mass spectra changes dramatically as the beam energy is increased. At 1.04 GeV, the pd cross section has a different mass dependence and is nearly an order of magnitude greater than the pp cross section. As the beam energy increases, the shape difference disappears and the pd cross section becomes approximately twice the pp cross section at all masses.

In Fig. 5 we show the pd/pp dielectron yield ratios as a function of mass for the six beam energies. These ratios were published previously [9]. These and all other yield ratios presented here are not corrected for the DLS acceptance since we found that the corrected ratios agreed with the uncorrected ratios to within the statistical uncertainties. Only the statistical uncertainties are included in the vertical bars in this figure. The overall normalization uncertainties on the pd/pp ratio do not effect the shape of the ratio distribution and

are not displayed in this figure. The pd/pp ratio distributions as a function of transverse momentum and rapidity which follow are also displayed in this format. Differences between the ratios presented here and those presented previously for the same data set [9] are smaller than the overall normalization uncertainties on the ratios.

The general trends of the mass dependence of the pd/pp ratio are reproduced by theories which contain mixtures of bremsstrahlung and hadron decay [31,42,43]. The increase in the pd/pp ratio as a function of increasing mass at the lower beam energies can be attributed to at least three mechanisms. First, since the largest possible pair mass is higher for the pd system than for the pp system due to Fermi momentum and coherence effects, there must be an enhancement in the pd/pp ratio at the pp kinematical limit [32]. The largest masses in the pp system are indicated by dashed lines in the figure. A second mechanism which has been proposed to explain the the mass dependence of the pd/pp ratio at the lower beam energies is interference between the bremsstrahlung and the Δ Dalitz decay contributions at high dielectron masses [31]. In the pp system this interference term is larger relative to the total dielectron cross section than in the pd system at low beam energies. This effect becomes less important as the beam energy is increased and additional dielectron production channels open up. A third mechanism which can cause the pd/pp ratio to increase as a function of mass is the η Dalitz decay contribution. The cross section for η production in the pn system is almost an order of magnitude greater than in the pp system near the η threshold of T=1.255 GeV [44], and the large pd/pp ratio at 1.27 GeV has been attributed to this effect [43]. The difference between η production in pp and pn collisions decreases as the beam energy increases [44], so the η Dalitz decay contribution is expected push the pd/pp ratio towards smaller values at the higher beam energies.

A comparison of the 1.04 GeV mass spectra with recently published data for d+Ca (dCa) at 1.0 A·GeV [50] is shown in Fig. 6. The shapes of the pd and dCa spectra are practically identical, but the pp spectrum drops off more quickly with mass than the dCa spectrum. This difference between the shapes of the pd and pp spectra is reflected in the increase of the pd to pp ratio as a function of mass discussed earlier. The dashed line in the figure

is from a fit to the dCa data using a model consisting of π° and sub-threshold η mesons only. The meson momentum distributions are assumed to be isotropic and thermal; for more details see Ref. [50]. The normalization of the π° and η Dalitz decay contributions are independently adjusted to fit the dCa data. The calculation provides a satisfactory match to both the the dCa and pd mass spectra shapes.

These comparisons suggest that the large pd/pp ratio at T=1.04 GeV might be due to sub-threshold η in the pd system. In order to further investigate this possibility, we compared the the difference between the pd and pp dielectron cross sections with a theoretical calculation of the η contribution. The mass dependence of the resulting spectrum was found to be very similar to that expected from η decay, but the inclusive η production cross section that was required to account for the difference between the pd and pp dielectron data was 240±60 μb. This is a large value relative to the measured η production cross sections near threshold [45]. Furthermore, a calculation of the η decay contribution at 1.0 GeV in the pd system including Fermi momentum of the deuteron and a short range nucleon-nucleon correlation concluded that the total cross section for eta production would be about 5 μb [43]. Thus it is unlikely that the entire enhancement of the pd cross section over that of the pp cross section can be explained by sub-threshold η production alone in the 1.04 GeV data.

Returning to Fig. 4, it is informative to note that the shape of the pp spectra changes abruptly as the beam energy goes over the threshold for η production at 1.27 GeV. This observation is consistent with theoretical calculations which indicate that η Dalitz decay should become the dominant source of low mass dielectrons ($m \leq 0.5$ GeV/c^2) in p-nucleus collisions as the beam energy is increased from 1 to 2 GeV [32]. The shape change is also apparent in the pd spectra.

At T=4.88 GeV, well above the 1.86 GeV threshold for production of the ρ and ω mesons, a peak appears in the mass spectra near the mass of these vector mesons. This peak is more prominent than in early presentations of the same data [8,10] since refinements of the DLS analysis procedures have improved the spectrometer's mass resolution. However, the mass resolution of the DLS spectrometer is still not sufficient to distinguish between

the contributions of the two vector mesons. There are at least three possible vector meson production mechanisms operating at this beam energy: production of ρ and ω mesons, $\pi - \pi$ annihilation [21,25], and VDM in bremsstrahlung and the decays of baryon resonances [31].

The widely assumed extension of VDM to the off-shell proton-virtual photon vertex has been predicted to produce enhancement in the mass spectra at the ρ mass for T=2.09 GeV [31,32]. The lack of a prominent vector meson peak in the 2.09 GeV mass spectra may provide information about the validity of extending VDM to the proton in this kinematic region. However, the degree to which the proton is off shell is predicted to affect the strength of the VDM form factor, weakening the magnitude of the enhancement at the ρ mass. The impact of this effect must be determined from the calculations of the strong-interaction T matrix [43,46,47]. Unfortunately, elastic nucleon-nucleon scattering does not provide enough guidance to determine the strong-interaction T matrix uniquely. It has therefore been suggested that a "cleaner" process for probing the form factor of the off-shell proton would be $\gamma + p \rightarrow p + e^+e^-$ which is purely electromagnetic [48].

B. Transverse Momentum and Rapidity Spectra

Transverse momentum spectra for pairs with masses greater than 0.15 GeV/c^2 are shown in Fig. 7, with the open and filled symbols denoting the pp and pd systems respectively. The standard bin width is 50 MeV/c, however some of the bins have been enlarged and these are plotted with horizontal bars. Excluding masses less than 0.15 GeV/c^2 primarily removes the contribution from π^0 Dalitz decay. These pairs would contribute to the cross section in the low $p_\perp$ region for all of the beam energies studied. This is demonstrated in in Fig. 8 which shows the 1.04 GeV pd data with and without the low mass contribution. This effect is primarily due to the DLS acceptance which restricts the contribution of π^0 Dalitz and other low mass pairs to low $p_\perp$ because of their small dielectron opening angles. See Ref. [10] for a detailed study of the relationship between the mass and transverse momenta spectra for the high statistics 4.88 GeV pp and pd data.

The shapes of the pd and pp spectra in Fig. 7 are generally featureless and quite similar to one another. This is also apparent in the pd/pp yield ratios which are shown in Fig. 9 as a function of $p_\perp$. Again, pairs with masses less than 0.15 GeV/c^2 have been excluded from the plot.

The laboratory rapidity dependence of the cross section for masses greater than 0.15 GeV/c^2 is shown in Fig. 10. The position of the arrows indicates mid-rapidity for each pp system. The low mass π^0 Dalitz decay pairs would primarily contribute to the highest rapidities, again due to the spectrometer acceptance. This is demonstrated for the 1.04 GeV pd data set in Fig. 11 which is displayed with and without the low mass contribution. This concentration of the low mass pairs at high rapidities is present in all of the data sets since it is primarily an acceptance effect.

As was the case for the $p_\perp$ spectra, the shapes of the rapidity spectra for the pd and pp spectra are similar. The pd/pp yield ratios are shown in Fig. 12 as a function of rapidity. As in Fig. 10, pairs with masses less than 0.15 GeV/c^2 have been excluded from the ratio plot.

The mass equivalence of the target and projectile in the pp system allows one to assume that the cross section must be symmetric around mid-rapidity. We have exploited this assumption in Fig. 13 and reflected the measured pp rapidity cross section around mid-rapidity for pairs with mass greater than 0.25 GeV/c^2. A higher value was chosen for the mass cut than in the previous plots in order to reduce the rapidity dependence of the DLS acceptance region. Although the acceptance still has a strong effect on the shape of the rapidity spectra, the data suggest a peak at mid-rapidity. This is seen most unambiguously in the 4.88 GeV data set.

C. Integrated Cross Sections

The integrated cross section for masses above 0.15 GeV/c^2 are shown in Fig. 14. The filled and open points denote the pd and pp systems respectively. The error bars indicate

the statistical uncertainties while the brackets above and below the points represent the systematic normalization uncertainties added linearly with the statistical errors. The cross section increases rapidly with increasing beam energy. Similar behavior was noted for the pBe dielectron cross section over the same energy range [35] and was described as a threshold-like phenomenon. Using this language, one could say that the pd system crosses over the threshold at a lower beam energy than pp. No doubt the additional energy available in the pd system due to the Fermi momentum of the deuteron plays a role.

In Ref. [50] the dielectron cross section in nucleus-nucleus collisions at T=1.0 A·GeV was found to scale as $\approx A_{proj} \times A_{targ}$ where A is the mass number. We found that the d+Ca, He+Ca, C+C, and Ca+Ca dielectron cross sections were well described by the function $\sigma = a(A_{proj}A_{targ})^b$ with a=0.017±0.010 μb and b=1.05±0.11 for the mass range 0.1 GeV/c^2 $\leq$m$\leq$ 0.35 GeV/c^2. This equation predicts 0.017±0.010 μb and 0.035±0.021 μb for pp and pd. These values are consistent with our measured values of 0.014±0.003 μb and 0.061±0.014 μb for the pp and pd cross sections in this mass region. The errors on the measured values were taken from systematic normalization uncertainties.

We show in Fig. 15 the pd/pp yield ratios for pairs with masses greater than 0.15 GeV^2 as a function of beam energy. These ratios were published previously [9]. In the previous publication, a ratio was presented for masses less than 0.10 GeV^2. We are not presenting this ratio in the current analysis because of the change in the DLS acceptance due to the cut on the minimum angle with respect to the beam. The error bars indicate the statistical uncertainties while the brackets above and below the points represent the systematic normalization uncertainties added linearly with the statistical errors. In the previous publication the systematic uncertainties in the ratios were specified in the text but not shown on the figure. The pd/pp ratio decreases as a function of beam energy as was discussed earlier.

IV. SUMMARY AND CONCLUSIONS

We have presented differential cross sections as a function of mass, transverse momentum, and rapidity for pp and pd collisions from T=1.04 to 4.88 GeV. The integrated cross section is found to be rapidly increasing with beam energy from T=1.04 to 4.88 GeV, as was also found to be the case in our previous studies of the pBe system. The shape of the mass spectra from pp collisions changes as the beam energy crosses over the threshold for η meson production, indicating the importance of the η Dalitz decay component. The shape of the pd mass spectrum at 1.04 GeV is found to be nearly identical to that of dCa at 1.0 A·GeV, but the pp mass spectrum falls off much more rapidly with increasing mass. At 4.88 GeV we observe a clear peak at the ρ-ω mass, but there is no obvious indication of a similar peak at 2.09 GeV. This may indicate a breakdown of VDM, but the interpretation is complicated by uncertainty in the strong interaction T matrix which can modify the shape of the mass spectrum.

The rapidity spectra for the pp collisions reflected about mid-rapidity suggests that the cross section for dileptons with masses greater than 0.25 GeV/c^2 peaks at mid-rapidity, particularly for the highest beam energies. The shapes of the transverse momentum and rapidity spectra for pp and pd collisions are similar. The contribution from π^0 Dalitz decays appears primarily at low transverse momentum and high rapidities within our acceptance.

The pd/pp ratio decreases with increasing beam energy. This indicates that although the dielectron production cross section in pp and pn collisions at 4.88 GeV are nearly equivalent, there is a large enhancement of pd relative to pp at the lower beam energies. This asymmetry has been attributed to the additional energy available in the pd system due to its Fermi momentum, destructive interference between dileptons created from bremsstrahlung and Δ Dalitz decay in the pp system at high mass, and, in the case of the 1.27 GeV data, the observed enhancement in η cross section in pn collisions relative to that of pp collisions near the η production threshold.

This data should provide a useful test of theoretical predictions of the relative importance

of various dielectron sources in the following manner. At 1.04 GeV in the pp system, only Δ Dalitz decay and pp bremsstrahlung are expected to contribute. Of the two, the Δ Dalitz decay is consistently predicted to dominate the dilepton production in this system. As the Δ production cross section is constrained by pion measurements [49], this system should provide a first test of the various bremsstrahlung calculations. If Δ decay is found to account for the pp data, the next test would be pd at 1.04 GeV. This should provide a stronger test of the bremsstrahlung models since they predict that bremsstrahlung will dominate here. The possible contribution of sub-threshold η production could be a complicating factor, but substantial body of data for η production near threshold exists. The trend in the pp and pd data as the beam energy is increased over the η threshold should provide additional tests of the η contribution. The comparison should then be extended to T=2.1 GeV where models which utilize the VDM form factor in the virtual photon to proton interaction predict an enhancement or shoulder at the ρ mass. Finally, the proposal that decays of heavy baryon resonances will produce ρ mesons with reduced masses due to phase space limitations which will fill in the dilepton cross section between the η and ρ mass can be tested in the evolution of the dilepton cross section from T=2.09 to the 4.88 GeV. The transverse momentum and rapidity spectra should provide additional constraints, so the comparisons should not be limited to the mass spectra alone. Once a model adequately reproduces the pp and pd data, it may be used to investigate the latest DLS nucleus-nucleus data [50] to search for any deviations from simple superposition of free hadron-hadron interactions caused be the presence of the nuclear medium.

ACKNOWLEDGMENTS

The authors appreciate the help from L. Bergstedt, J. Cailiu, W.B. Christie, L. Dean, N. Eddy, J. Kounas, B. Luttrell, D. Miller, L. Risk, and J. Ryans during the experimental setup, runs, and data analysis. We thank Al Smith for performing the beam ion chamber calibrations. We appreciate the effort from the Bevalac staff in support of this program. WKW

thanks Tom Cormier, Rene Bellwied, and the Wayne State University Physics Department for their support. This work was supported by the Director, Office of Energy Research, Office of High Energy and Nuclear Physics, Nuclear Physics Division of the U.S. Department of Energy under contracts No. DE-AC03-76SF00098, No. DE-FG03-88ER40424, No. DE-FG02-88ER40413.

REFERENCES

* Present address: Physics Dept., North Carolina Agricultural and Technical State University, Greensboro, NC 27411, USA.

† Present address: Lawrence Berkeley National Laboratory, University of California, Berkeley, CA 94720, USA.

‡ Present address: Max-Planck-Institut für Physik, München, Deutschland.

§ Present address: Brookhaven National Laboratory, Upton, NY 11973, USA.

Present address: Physics Dept., University Of California, Los Angeles, CA 90024 USA.

** Present address: Université de Paris VI et VII, LPNHE 75252 Paris Cedex 05, France.

†† Present address: Physics. Dept., Michigan State University, East Lansing, MI 48824, USA.

‡‡ Present address: JPL, Pasadena, California 91109, USA.

§§ Present address: Physics Dept. University of Michigan, Ann Arbor, MI 48109, USA.

Present address: Physics Division, CEBAF, Newport News, VA 23606, USA.

[1] C. Gale and J. Kapusta, Phys. Rev. C **35**, 2107 (1987).

[2] L.H. Xia et al., Nucl. Phys. **A485**, 721 (1988).

[3] Gy. Wolf et al., Nucl. Phys. **A517**, 615 (1990).

[4] Gy. Wolf et al., Phys. Rev. C **43**, 1501 (1991).

[5] G. Roche et al., Phys. Lett. **B226**, 228 (1989).

[6] S. Beedoe et al., Phys. Rev. C. **47**, 2840 (1993).

[7] F. de Jong and U. Mosel, Phys. Lett. **B392**, 273 (1997).

[8] H.Z. Huang et al., Phys. Lett. **B297**, 233 (1992).

[9] W.K. Wilson et al., Phys. Lett. **B316**, 245 (1993).

[10] H.Z. Huang et al., Phys. Rev. C **49**, 314 (1994).

[11] H.S. Matis et al., Nucl. Phys. A **583**, 617 (1995).

[12] V. Černý, P. Lichard, and J. Pišuť, Acta Phys. Pol. **10**, 115 (1979); P. Lichard and J.A. Thompson, Phys. Rev. D **44**, (1991) 668.

[13] V.D. Toneev et al., Phys. Lett. **B287**, 302 (1992).

[14] C. Gale and J. Kapusta, Phys. Rev. C **40**, 2397 (1989).

[15] L. Xiong et al., Nucl. Phys. **A512**, 772 (1990).

[16] L.G. Landsberg, Phys. Rep. **128**, 301 (1985).

[17] L. Xiong et al., Phys. Rev. C **R1355**, 41 (1990).

[18] R. Rückl, Phys. Lett. **B64**, 39 (1976).

[19] P. Lichard, SUNY preprint SUNY-NTG-94-16 (1994).

[20] Zhang et al., preprint McGill/94-56, Int. J. Mod. Phys. E, in print (1997).

[21] K. Haglin and C. Gale, Phys. Rev. C **49**, 401 (1994).

[22] L.A. Winckelmann et al., Phys. Lett. **B298**, 22, (1993).

[23] K. Haglin and J. Kapusta, Phys. Lett. **B224**, 433 (1989).

[24] M. Schäfer et al., Phys. Lett. **B221**, 1 (1989).

[25] J. Kapusta and P. Lichard, Phys. Rev. C. **40**, R1574 (1989).

[26] L.A. Winckelmann et al., Phys.Rev.C **51**, 9 (1995).

[27] T. Akesson et al., Zeit. Phys. **C68**, 47 (1995).

[28] G. Bardin et al., Phys. Lett. **B255**, 149 (1991).

[29] G. Bardin et al., Phys. Lett. **B257**, 514 (1991).

[30] Gy. Wolf et al. Nucl. Phys. **A552**, 549 (1993).

[31] M. Schäfer et al., Nucl. Phys. **A575**, 429, (1994).

[32] B. Kämpfer et al., Phys. Lett. **B301**, 123 (1993).

[33] T. Akesson et al., Phys. Lett. **B152**, 411 (1985).

[34] A. Brownman et al., Phys. Rev. Lett. **37**, 246 (1976).

[35] C. Naudet et al., Phys. Rev. Lett. **62**, 2652 (1989).

[36] M. Bougteb, PhD Thesis (unpublished), A L'Universites Blaise Pascal - Clermont II, (1994).

[37] L.M. Lederman, Phys. Rep. C **28**, 149 (1976); N.S. Craigie, *ibid.* **47**, 1 (1978); R. Stroynowski, *ibid.* **71**, 1 (1981).

[38] G. Agakichiev et al., Phys. Rev. Lett **75**, 1272 (1995).

[39] A Yegneswaran et al., Nucl. Instr. and Meth. in Phys. Res. **A290**, 61 (1990).

[40] G. Roche et al., Phys. Rev. Lett. **61**, 1069 (1988).

[41] A. Letessier-Selvon et al., Phys. Rev. C **40**, 1513 (1989). J. Phys. **G15**, 437 (1989). Phys. Rev. D **48**, R2969 (1993).

[42] K. Haglin et al., Proceedings of the 9th High Energy Heavy Ion Study, Lawrence Berkeley Laboratory (1993), LBL-35984.

[43] A.I. Titov et al., Phys. Rev **C51**, 227 (1995).

[44] E. Chiavassa et al., Phys. Lett. **B337**, 192 (1994).

[45] H. Calén et al., Phys. Lett. **B366**, 39 (1996).

[46] H.C. Döenges, et al., Phys. Rev. C **51**, 950 (1995).

[47] F. de Jong and U. Mosel, Phys. Lett. **379**, 45 (1996).

[48] M. Schäfer et al., Phys. Lett. **B342**, 13 (1995).

[49] B.J. Ver West and R.A. Arndt, Phys. Rev. C25, 1979 (1982).

[50] R.J. Porter et al., Lawerence Berkeley National Laboratory preprint LBNL-39957, to be published in Phys. Rev. Lett. (1997).

[51] K.A. Jenkins et al., Phys. Rev. D **21**, 2445 (1980).

[52] R.C. Kammerud et al., Phys. Rev. D **4**, 1309 (1971).

[53] D.T. Williams et al., Nuovo Cimento **8A**, 447 (1972).

[54] Bratkovskaya et al., Phys. Lett. **B362**, 17 (1995).

APPENDIX A: PP ELASTIC SCATTERING STUDY

During the T=1.27 GeV running, we also acquired a sample of proton pairs for comparison with previous measurements of pp elastic scattering. This proton pair data allowed us to check of the DLS spectrometer and analysis software performance. The standard dielectron trigger requires hits in scintillator arrays in each arm as well as hits in the Čerenkov gas radiators to select electrons. In order to obtain hadron pairs during the pp elastic running, the Čerenkov gas radiators were omitted from the trigger. In all other respects the spectrometer setup and tracking software was identical to that of the dielectron runs.

Pion contamination was minimized using cuts on time-of-flight vs. momentum. Elasticly scattered proton pairs were selected by requiring that the two tracks be within 2° of coplanarity. The momentum transfer (t) was calculated for each pair. The geometrical acceptance of the spectrometer was calculated as a function of t and used to perform an acceptance correction of the data in a procedure similar to that used in the dielectron data. The normalization corrections for tracking efficiency and the count rate dependent trigger efficiency

were calculated and applied in the same manner as they were for the dielectron data. Since a wider range of count rates samples and higher statistics at each rate were available for the pp elastic studies than for the dielectron runs, the overall systematic uncertainty in the normalization of the pp elastic cross section was greatly reduced.

Our measurements (filled stars) for the acceptance corrected t distribution from pp elastic scattering events is shown in Fig. 16 for the 1.27 GeV system. The error bars shown are statistical only. This is compared with previous measurements at 1.25 GeV (open circles) [51] and 1.27 GeV (open squares and triangles) [53,52]. The excellent agreement implies that we have correctly estimated the various efficiencies and acceptance corrections for hadrons.

The similarities between the pp elastic analysis and the dielectron analysis confirm that there is no gross error in the techniques of the dielectron analysis. It does not test the correction for the Čerenkov detection efficiency, but this is a small factor when compared to the overall normalization uncertainties in the dielectron data.

We were also able to use the elastic scattering events to check the calibration of the spectrometer momentum scale. This involved the magnitude and shape of the magnetic field as well as the positions of the drift chamber wire planes. We found that the momentum of elasticly scattered protons was correctly reconstructed to within the expected resolution of the spectrometer.

APPENDIX B: ACCEPTANCE CORRECTION

The correction for the DLS acceptance is intimately tied to the manner in which the cross sections are reported, so we will begin by considering the options available in presenting the data. In the following, we will refer to the region in which the DLS is able to reliably report cross sections as the acceptance region.

Since each electron pair requires six variables to specify its kinematics, the acceptance region of the DLS forms a volume in a six dimensional space determined by the geometry of the spectrometer. Within this hyper-surface, the acceptance is 100 %, but it drops rapidly

to 0 % outside the surface. An example of a six-variable set which spans the space is the Cartesian components of the 3-momenta of the electrons. Another example more closely tied to the kinematics of the parent virtual photon is the set (m,$p_\perp$,y,ϕ,$\phi_{\rm pol}$,$\theta_{\rm pol}$). The variables m, $p_\perp$, y, and ϕ refer to the mass, transverse momentum, rapidity, and azimuthal angle of the parent. The polarization angles $\phi_{\rm pol}$ and $\theta_{\rm pol}$ are the azimuthal and polar angles of one of the electrons with respect to the plane defined by the beam axis and the momentum vector of the virtual photon. After measuring the cross section within this volume, one may proceed to project the data onto a single axis without any further acceptance correction. Any theory which is to be compared with the data would have to be generated in the six dimensional space and filtered, keeping the pairs which lie within the DLS acceptance region and rejecting those that lie outside the acceptance. Then the projections of the measured cross sections and of the filtered theory could be compared.

There are several drawbacks to this approach. It would be impossible to specify the six dimensional hyper surface bounding the DLS acceptance region without imposing artificial cuts which would drastically reduce the pair sample statistics. Alternately, a six dimensional grid described by a lookup table would be impractical due to the enormous space required to store such a table. In addition, the data is extremely sparse when binned in six dimensions, leading to problems in the extraction of cross sections.

Fortunately, it is not necessarily useful to keep track of all six variables since some of them carry limited information about the physics of the parent virtual photon. For example, the azimuthal angle of the virtual photon about the beam axis is meaningless without a technique for characterizing the azimuthal angle of the reaction plane or the polarization of the beam. Since such information is not available, the parent distribution will be uniformly distributed over 360°. The acceptance of the DLS in $\phi_{\rm pol}$ is somewhat limited. For these reasons, the DLS group chooses to reduce the acceptance region to three variables by averaging the acceptance over the three angular variables with the assumption that the initial population of these variables was isotropic.

Compressing the six variable space to three variables makes the task of filtering the theory

tractable. However, it causes the acceptance within the three-dimensional acceptance region to deviate from 100 % due to incomplete acceptance in the three angular variables. In order to measure the loss in acceptance for each point in the three-dimensional space, we use GEANT simulations of the spectrometer's performance. For each bin in m, $p_\perp$, and y, we generate many pairs with isotropic distributions in the three angular variables and calculate the losses due to the detector geometry, creating a three-dimensional table of acceptance corrections. The edges of the acceptance are not sharp in the three-dimensional space, so we use an acceptance cutoff and other edge characterization tests to define the acceptance region. (In this paper, we set the lower limit on the acceptance to 0.001, *i.e.* we demand that at least one in a thousand pairs in a given m, $p_\perp$, and y bin are accepted, before we will present a cross section.) Following projection, we obtain a spectrum which reflects the cross section within the DLS acceptance region in three dimensional m-$p_\perp$-y space, under the assumption that both types of polarization are negligible.

In an arm, an electron may bend towards or away from the beam depending on the polarity of the magnetic field. Data was taken with all four magnet polarity combinations, leading to four pair geometries: both particles bending toward the beam, both bending away from the beam, left arm particle bending towards while the right arm particle bends away from the beam, and visa versa. The acceptance of the spectrometer is different for the four different pair geometries, especially at low invariant mass. In our previous publications, the acceptance region was defined by the average of the acceptance over the four pair geometry types. For the current data set we quote the cross section of a given m-$p_\perp$-y bin if there is at least one pair geometry which has a sufficiently large acceptance. This choice slightly reduces but does not eliminate the impact of the DLS acceptance on the shape of the mass spectra at low invariant masses. More importantly, the new treatment of the acceptance boundaries provides a more accurate characterization of the DLS cross sections. The data from the four pair geometry types are combined using maximum-likelihood techniques.

The assumption that the distributions in the polarization angles are flat introduces little if any bias in the acceptance correction. Even if the polarization is strong $[1.0 \pm \cos^2(\theta_{pol})]$

the overall error in the acceptance is $\leq 15.0\%$. However, recent publications have suggested that the polarization angle distributions may be useful in disentangling the various dielectron sources [54]. We are currently investigating new techniques for filtering theoretical polarization angle predictions to see if any meaningful comparison can be made with the DLS data.

TABLES

TABLE I. Summary of DLS hydrogen target running periods

Date	Beam Energies (GeV)
September 1990	4.88
August 1991	1.04, 1.61, 2.09
June 1992	1.27, 1.85, 4.88

TABLE II. Overall systematic normalization uncertainties by system.

Beam Energy (GeV)	pp	pd	pd/pp
1.04	±23%	±23%	±32%
1.27	±22%	±30%	±37%
1.61	±23%	±23%	±32%
1.85	±23%	±23%	±32%
2.09	±23%	±23%	±32%
4.88	±15%	±12%	±19%

FIGURES

FIG. 1. The magnitudes of the combinatoric background are shown in arbitrary units for the pd system at 1.04 and 4.88 GeV. The circles denote the opposite-sign (OS) mass spectra, the crosses denote the opposite sign background (OSBK) spectra generated from the like-sign (LS) pairs via event mixing, and the solid histograms denote the true pair spectra (true samples).

FIG. 2. The measured like-sign (LS) mass spectra (circles) are shown in arbitrary units along with the generated LS spectra (crosses). This comparison tests the event mixing procedure for the pd system at 1.04 and 4.88 GeV.

FIG. 3. The uncorrected true pair mass spectra (circles) are compared with the acceptance corrected spectra (crosses). The uncorrected yield has been multiplied by a factor of 100 to facilitate the comparison.

FIG. 4. Acceptance-corrected mass spectra for the pd (filled circles) and pp (open circles) systems. The error bars are statistical and do not include the normalization uncertainties shown in Table II. The brackets above and below the low mass data points indicate systematic uncertainties in the shape of the spectra. The dashed lines indicate the kinematical upper limit on the pair mass in the pp system. Note that the finite mass resolution of the DLS allows reconstructed masses to exceed this limit.

FIG. 5. The ratio of the dielectron yields in the pd and pp systems presented as a function of mass. The dashed lines indicate the kinematical upper limit on the pair mass in the pp system. Note that the vertical scale changes for the bottom row.

FIG. 6. The shapes of the acceptance-corrected mass spectra for the pd (filled squares) and pp (filled circles) systems at 1.04 GeV are compared to a mass spectrum from d+Ca (open squares) at 1.0 A·GeV. The pd and pp cross sections have been multiplied by 28 and 110 respectively. The fit is described in the text. The d+Ca data [50] and the fit are taken from Porter et al.

FIG. 7. Acceptance-corrected transverse momentum spectra for the pd (filled circles) and pp (open circles) systems. Only pairs with masses greater than 0.15 GeV/c^2 are included. The error bars do not include the normalization uncertainties shown in Table II. The brackets above and below the low transverse momentum data points indicate systematic uncertainties in the shape of the spectra.

FIG. 8. Acceptance-corrected transverse momentum spectra from the 1.04 GeV pd system with (crosses) and without (circles) the contribution from pairs with masses less than 0.15 GeV/c^2.

FIG. 9. The ratio of the dielectron yields in the pd and pp systems are presented as a function of transverse momentum. Only pairs with masses greater than 0.15 GeV/c^2 are included. Note that the vertical scale changes for each row.

FIG. 10. Acceptance-corrected laboratory rapidity spectra for the pd (filled circles) and pp (open circles) systems. Only pairs with masses greater than 0.15 GeV/c^2 are included. Arrows are used to indicate the position of mid-rapidity for each system. The error bars do not include the normalization uncertainties shown in Table II. Note that the vertical scale changes for each panel.

FIG. 11. Acceptance-corrected laboratory rapidity spectra from the 1.04 GeV pd system with (crosses) and without (circles) the contribution from pairs with masses less than 0.15 GeV/c^2.

FIG. 12. The ratio of the dielectron yields in the pd and pp systems are presented as a function of laboratory rapidity. Only pairs with masses greater than 0.15 GeV/c^2 are included. Note that the vertical scale changes for each row.

FIG. 13. Acceptance-corrected laboratory rapidity spectra from the pp system measured (circles) and reflected around mid-rapidity (crosses). A pair mass lower limit of 0.25 GeV/c^2 was imposed to reduce the rapidity dependence of the acceptance. Arrows are used to indicate the position mid-rapidity for each system. Note that the vertical scale changes for each panel.

FIG. 14. Acceptance-corrected integrated cross section for masses greater than 0.15 GeV/c^2 are shown as a function of the beam energy for the pd (filled) and pp (open) systems. The error bars are statistical while the brackets above and below the points include the effects of the normalization uncertainties.

FIG. 15. The ratio of the dielectron yields in the pd and pp systems are presented as a function of beam energy. Only pairs with masses greater than 0.15 GeV/c^2 are included. The error bars are statistical while the brackets above and below the points include the effects of the normalization uncertainties.

FIG. 16. The acceptance corrected momentum transfer (t) distribution from pp elastic scattering events for the 1.27 GeV system (filled stars). This is compared with previous measurements at 1.25 GeV (open circles) and 1.27 GeV (open squares and triangles).

figure 1

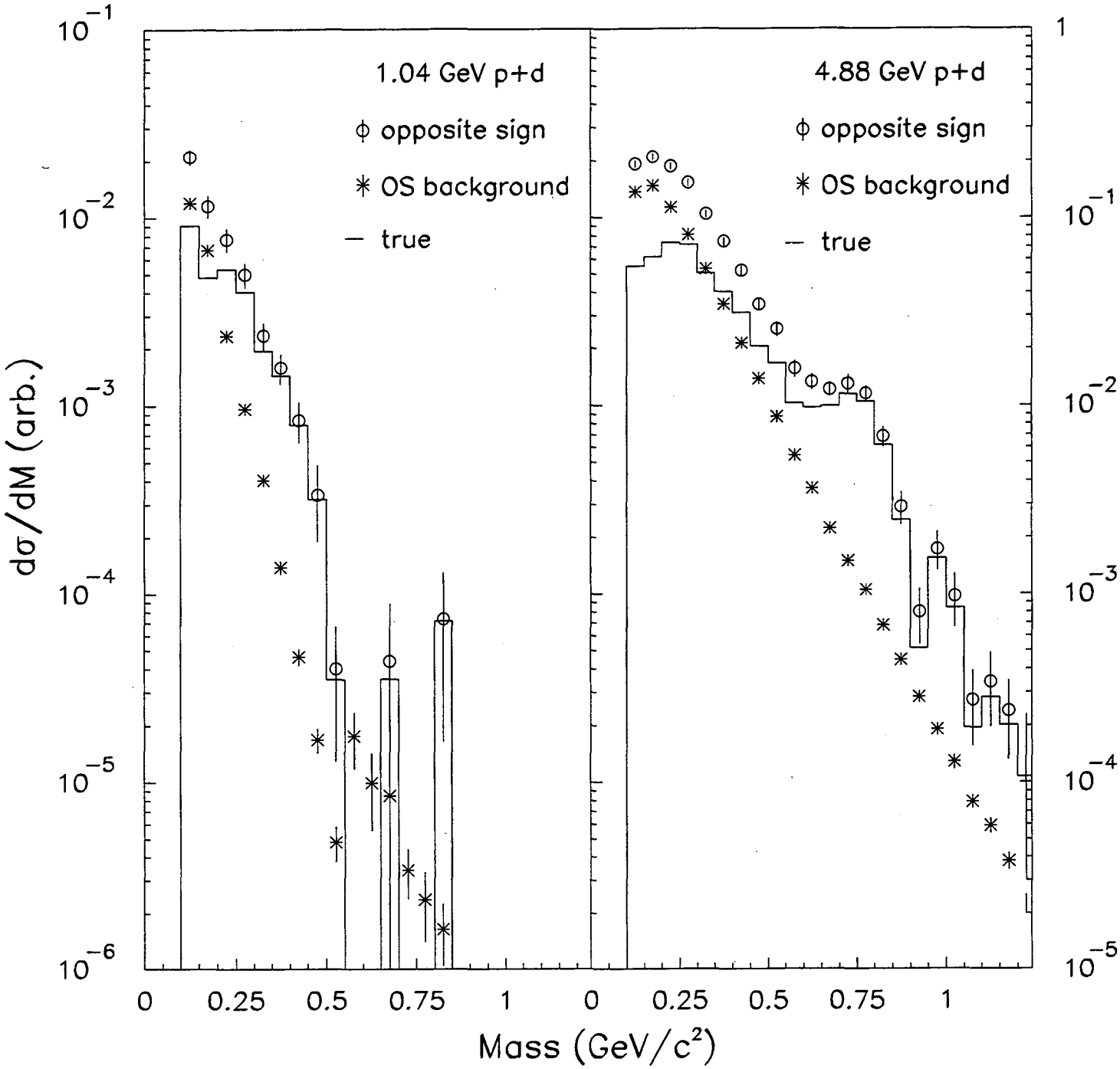
1.04 GeV p+d
ϕ opposite sign
OS background
true
4.88 GeV p+d
ϕ opposite sign
OS background
true
dσ/dM (arb.)
Mass (GeV/c²)
10⁻¹
10⁻²
10⁻³
10⁻⁴
10⁻⁵
10⁻⁶
1
0
0.25
0.5
0.75
1

figure 2

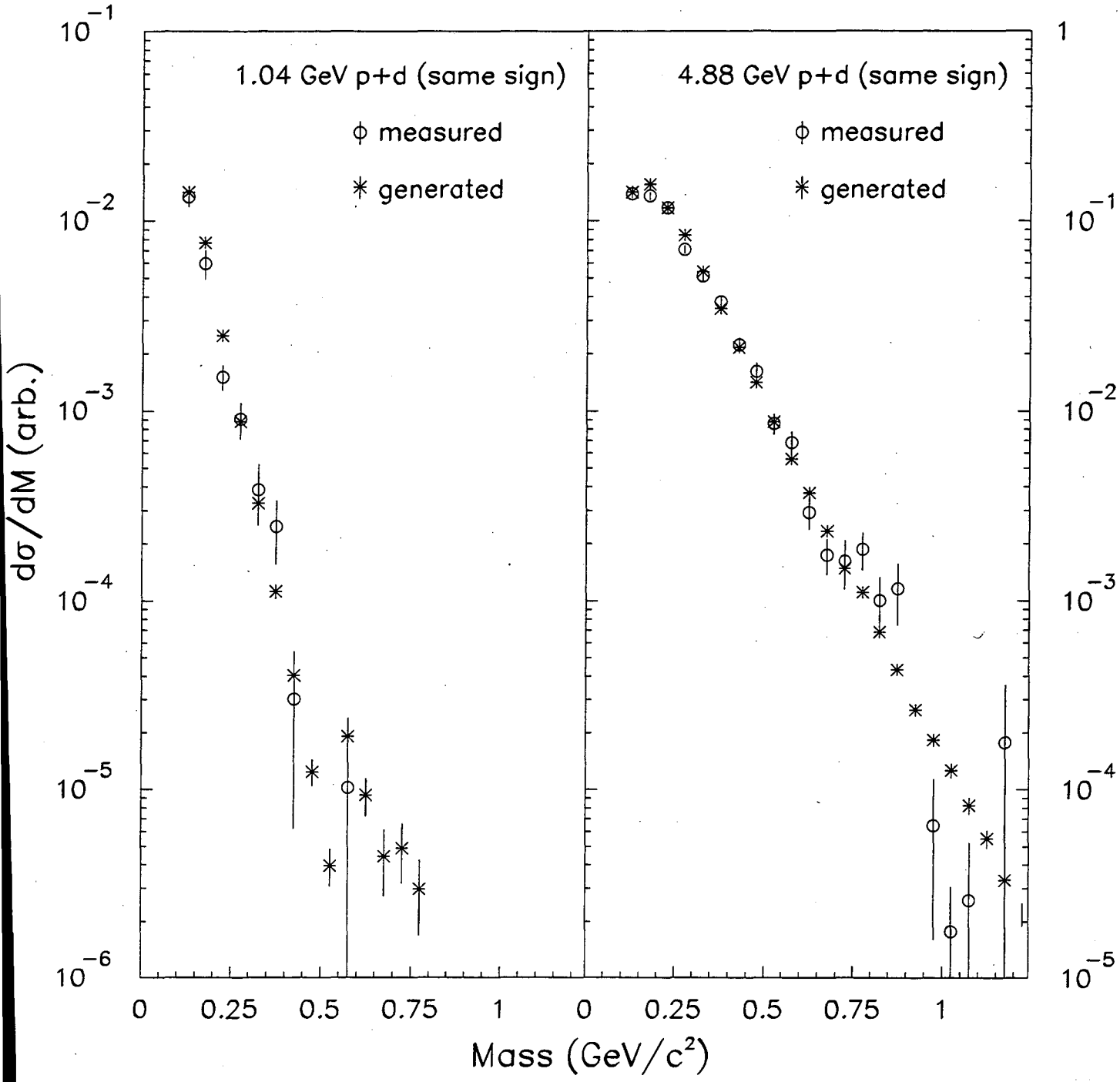
1.04 GeV p+d (same sign)
ϕ measured
generated
4.88 GeV p+d (same sign)
ϕ measured
generated
dσ/dM (arb.)
Mass (GeV/c²)
10⁻¹
10⁻²
10⁻³
10⁻⁴
10⁻⁵
10⁻⁶
1
0
0.25
0.5
0.75
1

figure 3

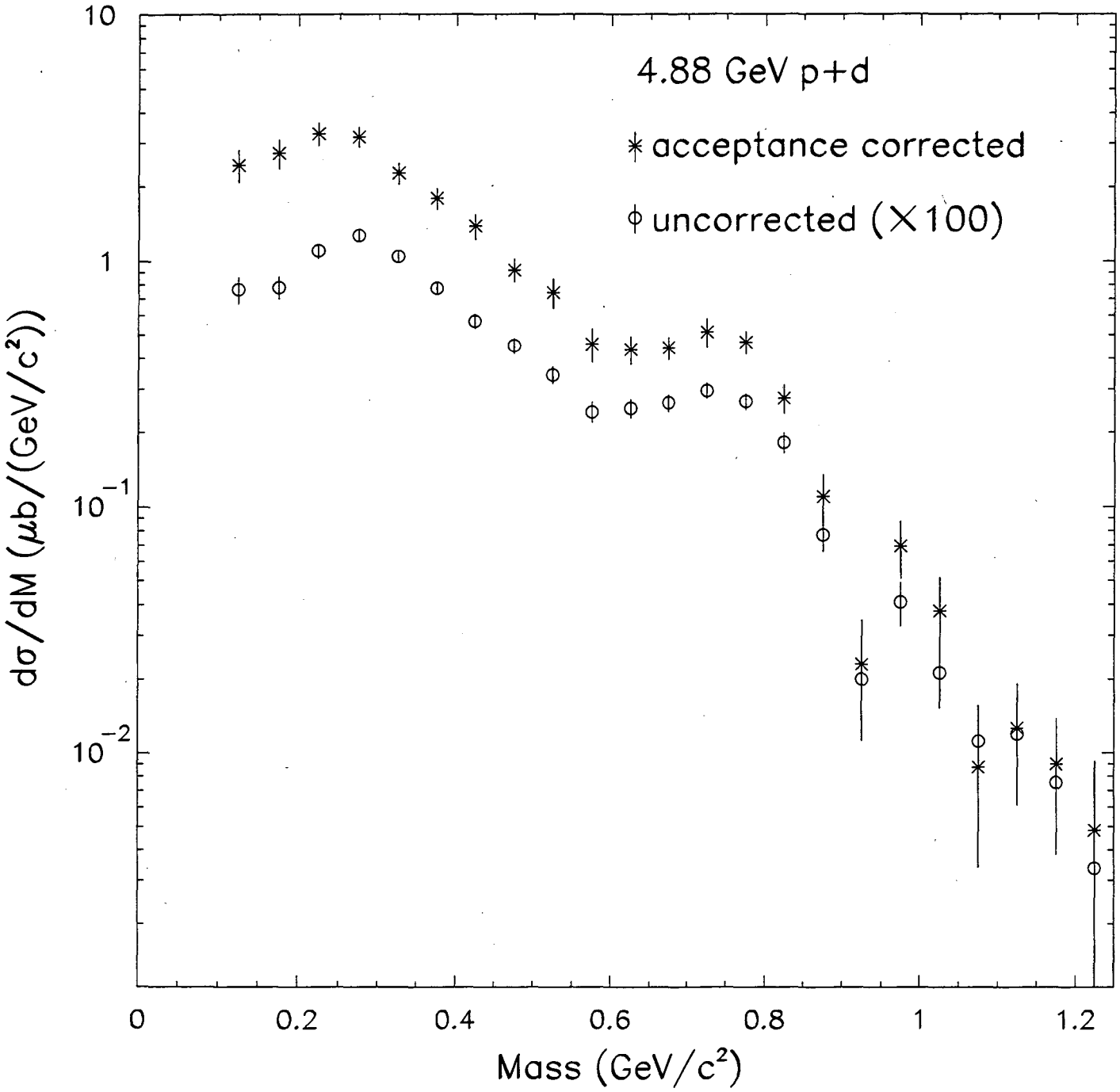
4.88 GeV p+d
acceptance corrected
uncorrected (×100)
dσ/dM (μb/(GeV/c²))
Mass (GeV/c²)
10
1
10⁻¹
10⁻²
0
0.2
0.4
0.6
0.8
1
1.2

figure 4

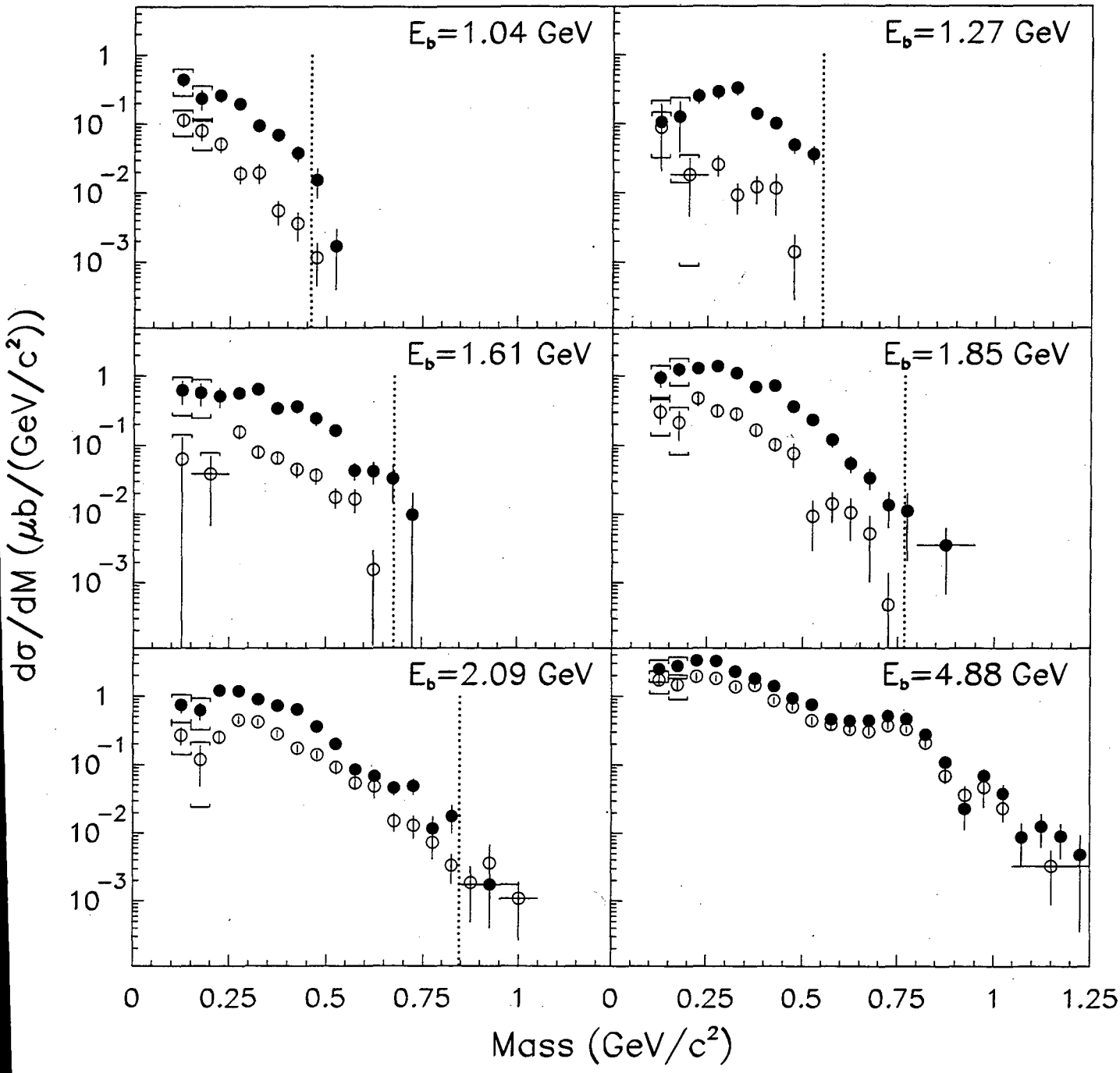
E_b=1.04 GeV
E_b=1.27 GeV
E_b=1.61 GeV
E_b=1.85 GeV
E_b=2.09 GeV
E_b=4.88 GeV
$d\sigma/dM$ ($\mu b/(GeV/c^2)$)
Mass (GeV/c^2)
1
10^{-1}
10^{-2}
10^{-3}
0
0.25
0.5
0.75
1
1.25

figure 5

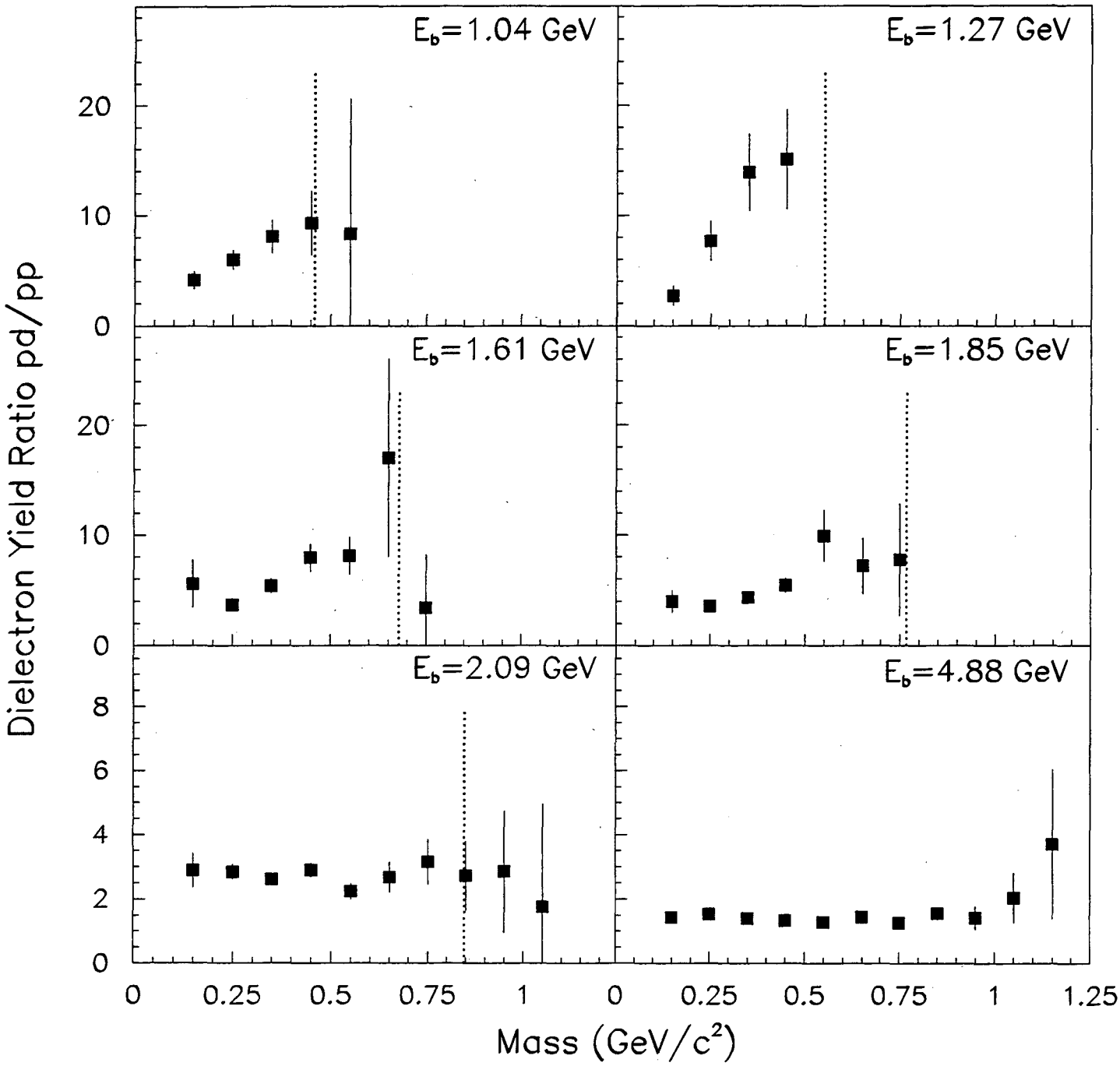
E_b=1.04 GeV
E_b=1.27 GeV
E_b=1.61 GeV
E_b=1.85 GeV
E_b=2.09 GeV
E_b=4.88 GeV
Dielectron Yield Ratio pd/pp
Mass (GeV/c^2)
0
10
20
2
4
6
8
0.25
0.5
0.75
1
1.25

figure 6

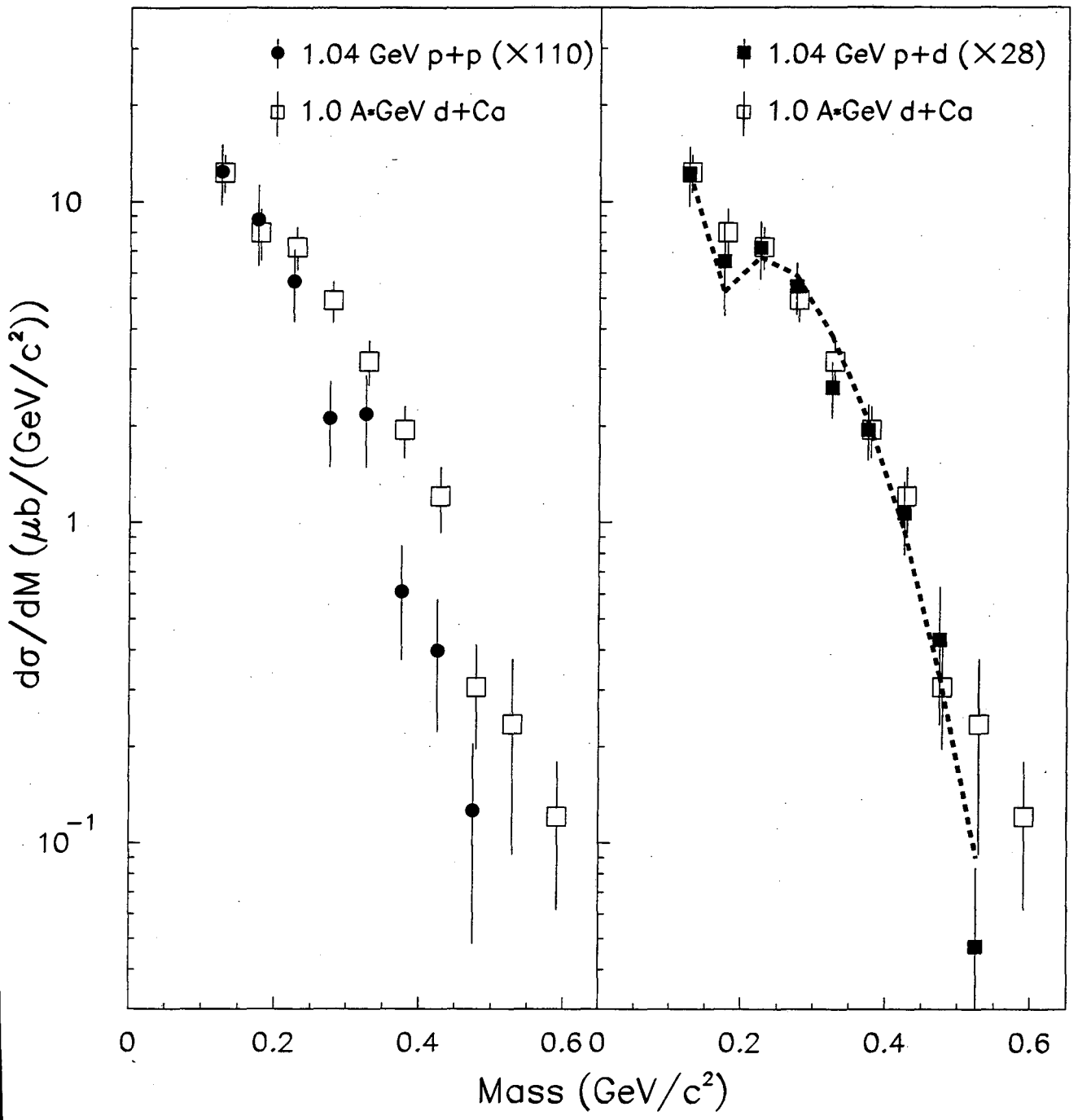
1.04 GeV p+p (×110)
1.0 A·GeV d+Ca
1.04 GeV p+d (×28)
1.0 A·GeV d+Ca
10
1
10^{-1}
dσ/dM (μb/(GeV/c²))
0
0.2
0.4
0.6
0
0.2
0.4
0.6
Mass (GeV/c²)

figure 7

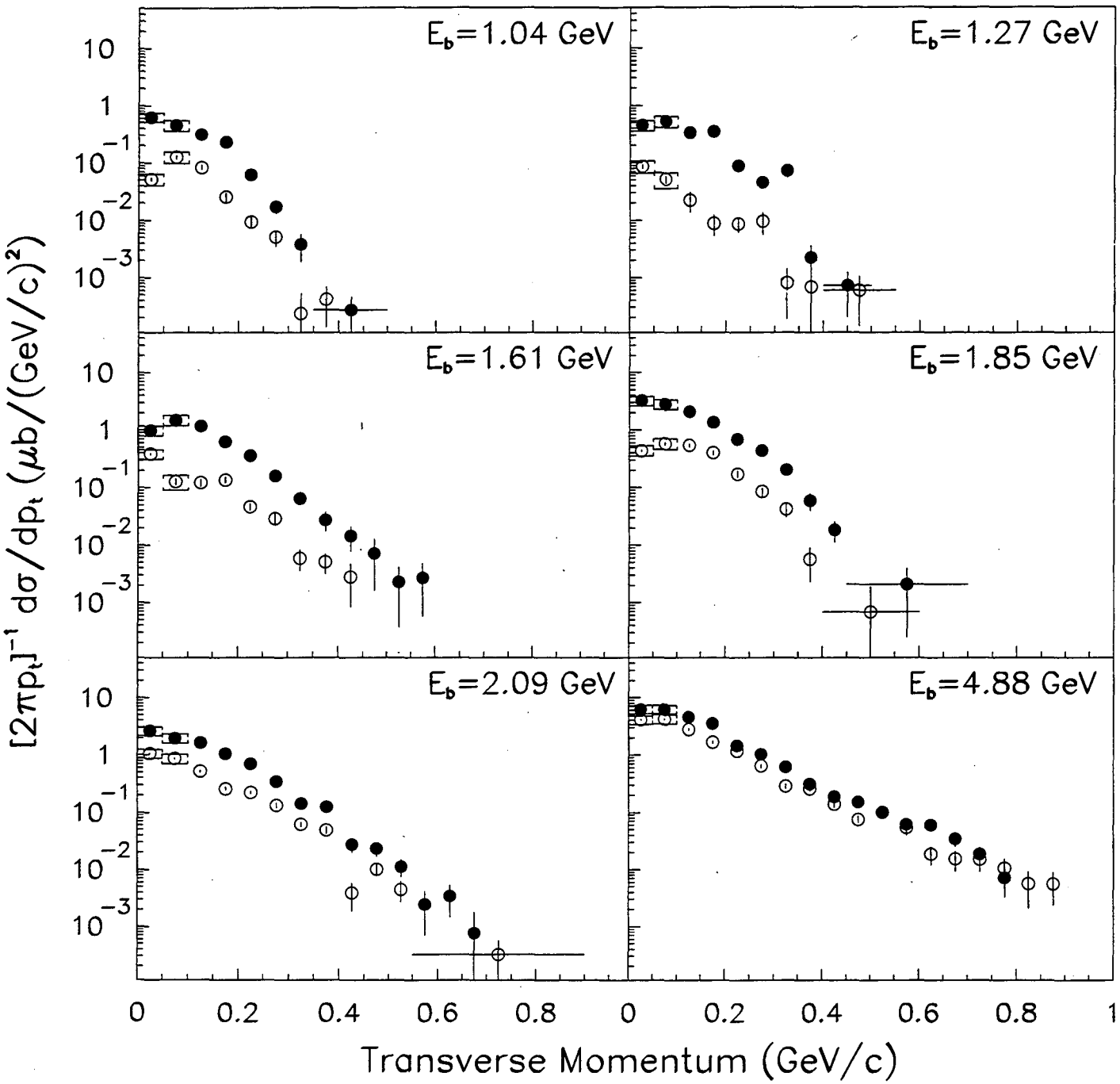
E_b=1.04 GeV
E_b=1.27 GeV
E_b=1.61 GeV
E_b=1.85 GeV
E_b=2.09 GeV
E_b=4.88 GeV
$[2\pi p_t]^{-1}\ d\sigma/dp_t\ (\mu b/(GeV/c)^2)$
Transverse Momentum (GeV/c)

figure 8

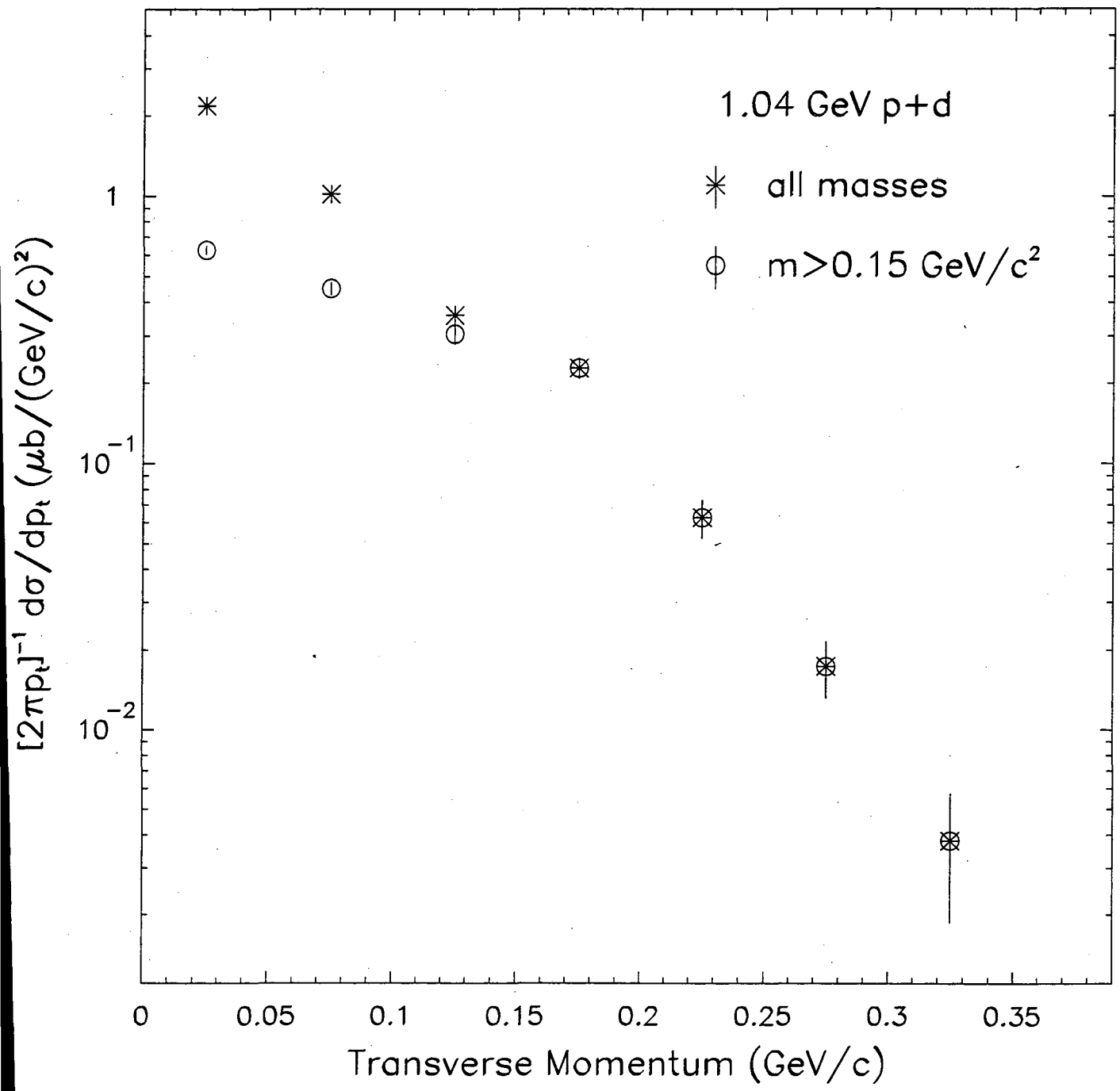
1.04 GeV p+d
all masses
m>0.15 GeV/c²
1
10⁻¹
10⁻²
[2πp_t]⁻¹ dσ/dp_t (μb/(GeV/c)²)
0
0.05
0.1
0.15
0.2
0.25
0.3
0.35
Transverse Momentum (GeV/c)

figure 9

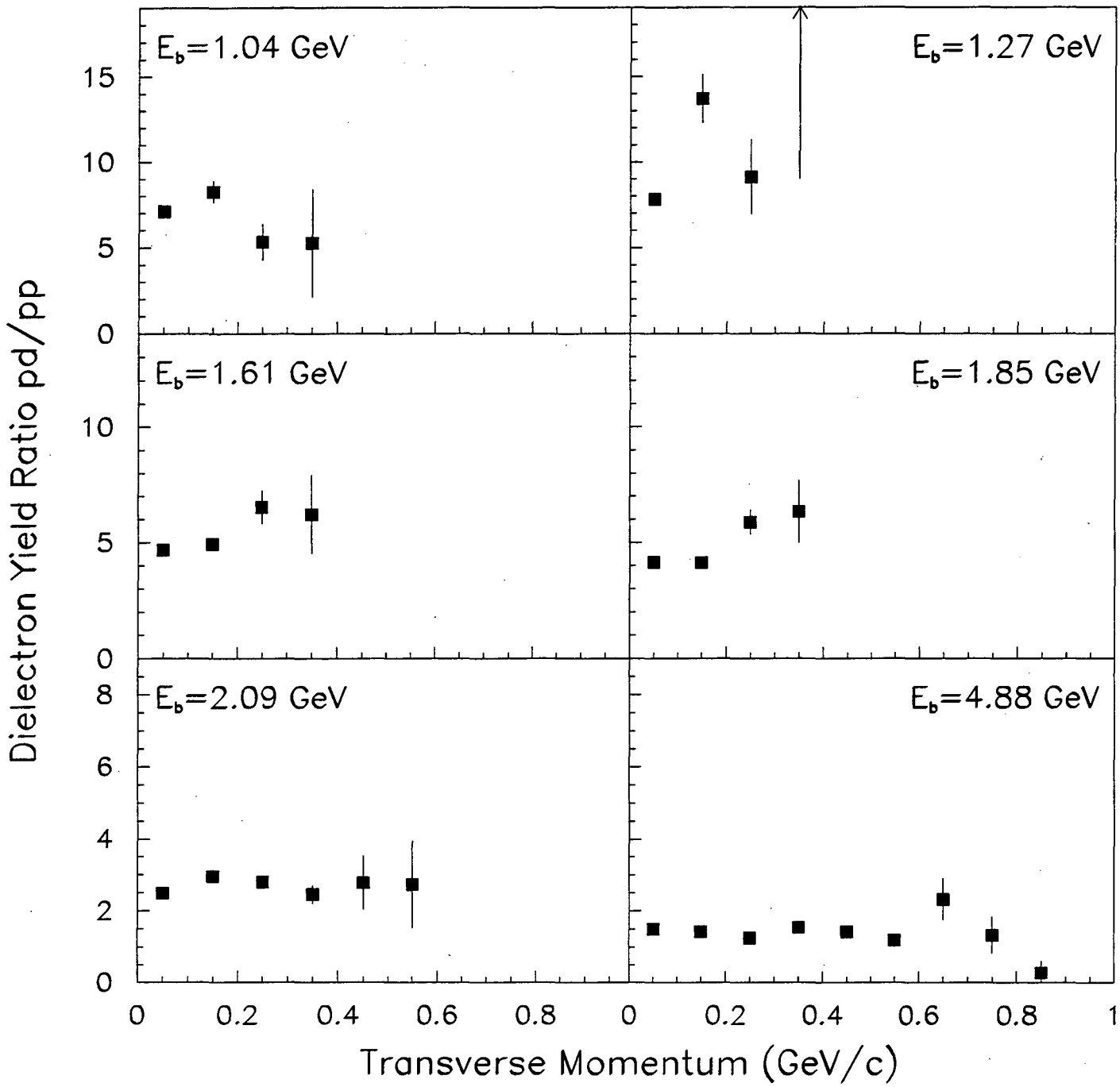
E_b=1.04 GeV
E_b=1.27 GeV
E_b=1.61 GeV
E_b=1.85 GeV
E_b=2.09 GeV
E_b=4.88 GeV
Dielectron Yield Ratio pd/pp
Transverse Momentum (GeV/c)
0
5
10
15
2
4
6
8
0.2
0.4
0.6
0.8
1

figure 10

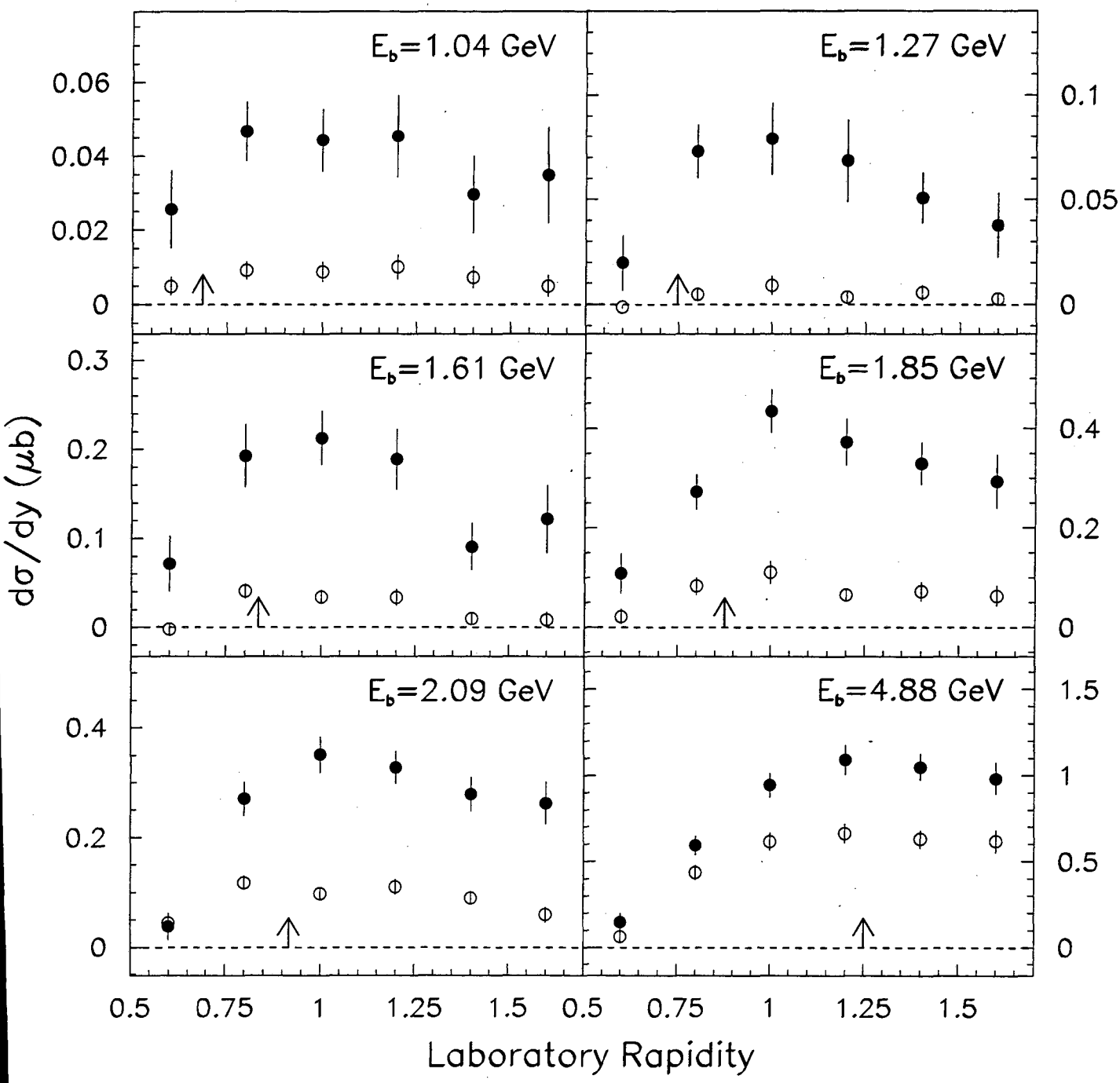
E_b=1.04 GeV
E_b=1.27 GeV
E_b=1.61 GeV
E_b=1.85 GeV
E_b=2.09 GeV
E_b=4.88 GeV
dσ/dy (μb)
Laboratory Rapidity
0.5
0.75
1
1.25
1.5

figure 11

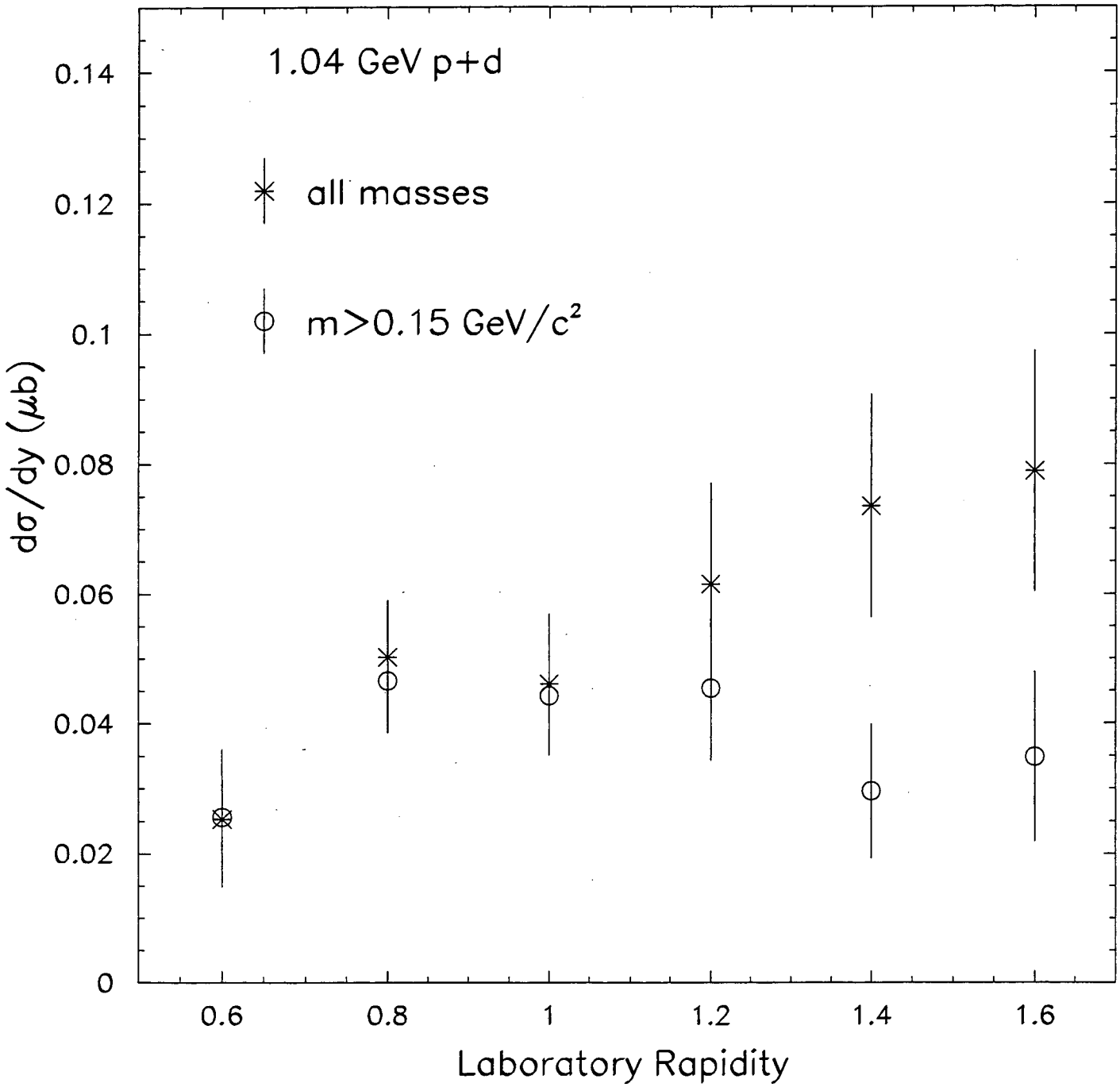
1.04 GeV p+d
all masses
m>0.15 GeV/c²
dσ/dy (μb)
0.14
0.12
0.1
0.08
0.06
0.04
0.02
0
0.6
0.8
1
1.2
1.4
1.6
Laboratory Rapidity

figure 12

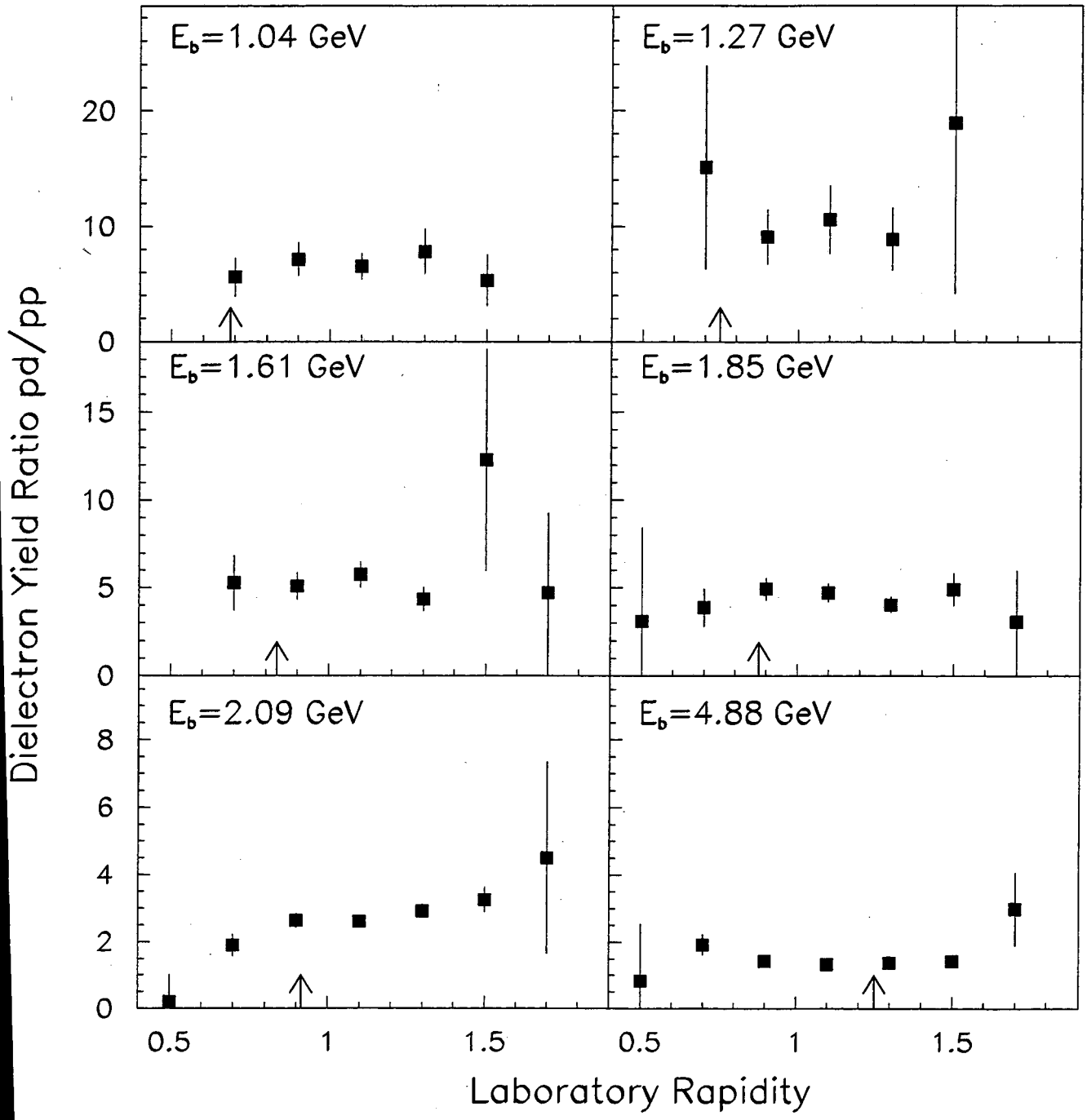
E_b=1.04 GeV
E_b=1.27 GeV
E_b=1.61 GeV
E_b=1.85 GeV
E_b=2.09 GeV
E_b=4.88 GeV
Dielectron Yield Ratio pd/pp
Laboratory Rapidity
0
10
20
5
15
2
4
6
8
0.5
1
1.5

figure 13

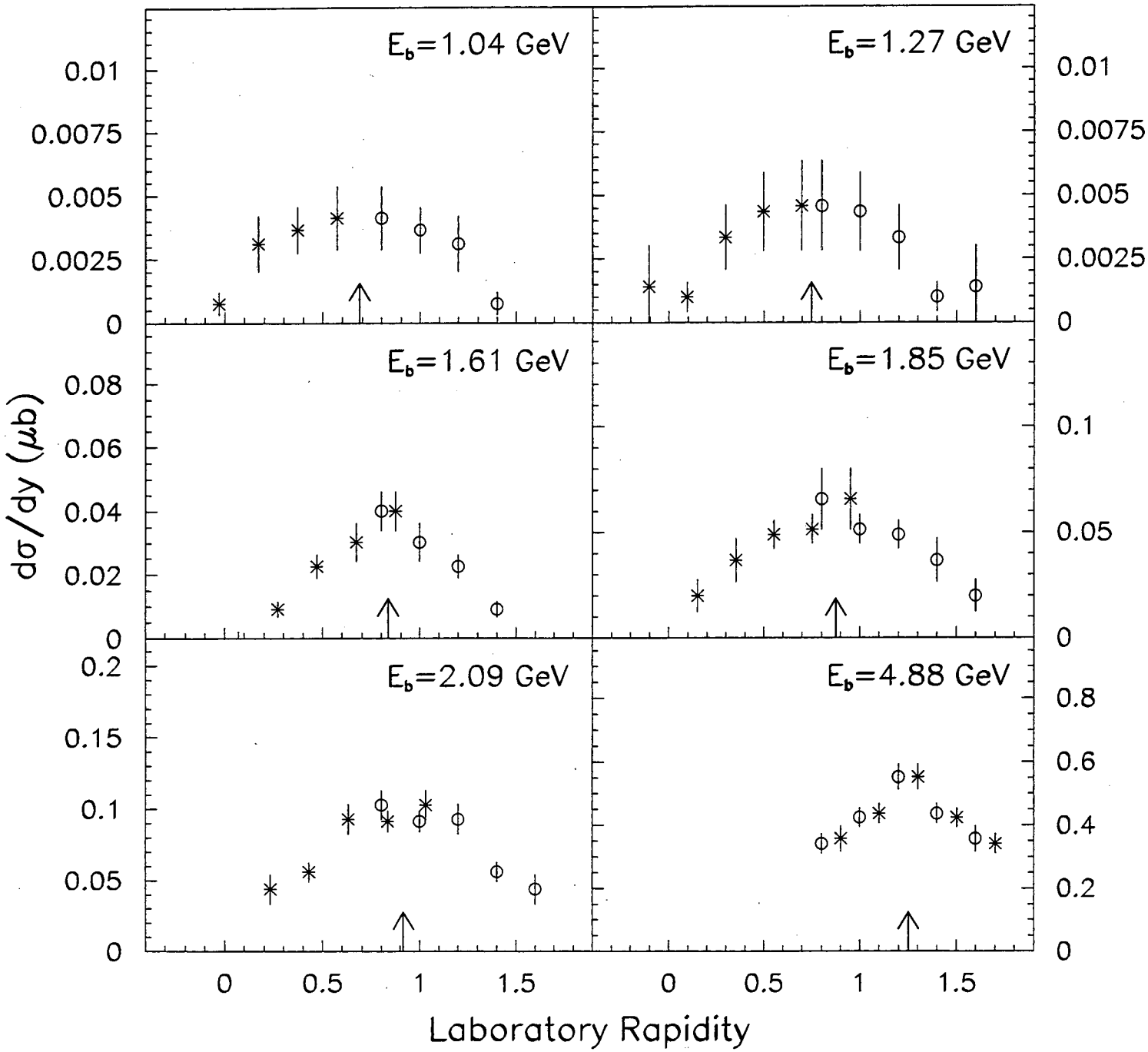
E_b=1.04 GeV
E_b=1.27 GeV
E_b=1.61 GeV
E_b=1.85 GeV
E_b=2.09 GeV
E_b=4.88 GeV
dσ/dy (μb)
Laboratory Rapidity
0
0.0025
0.005
0.0075
0.01
0.02
0.04
0.06
0.08
0.05
0.1
0.15
0.2
0.2
0.4
0.6
0.8
0.5
1
1.5

figure 14

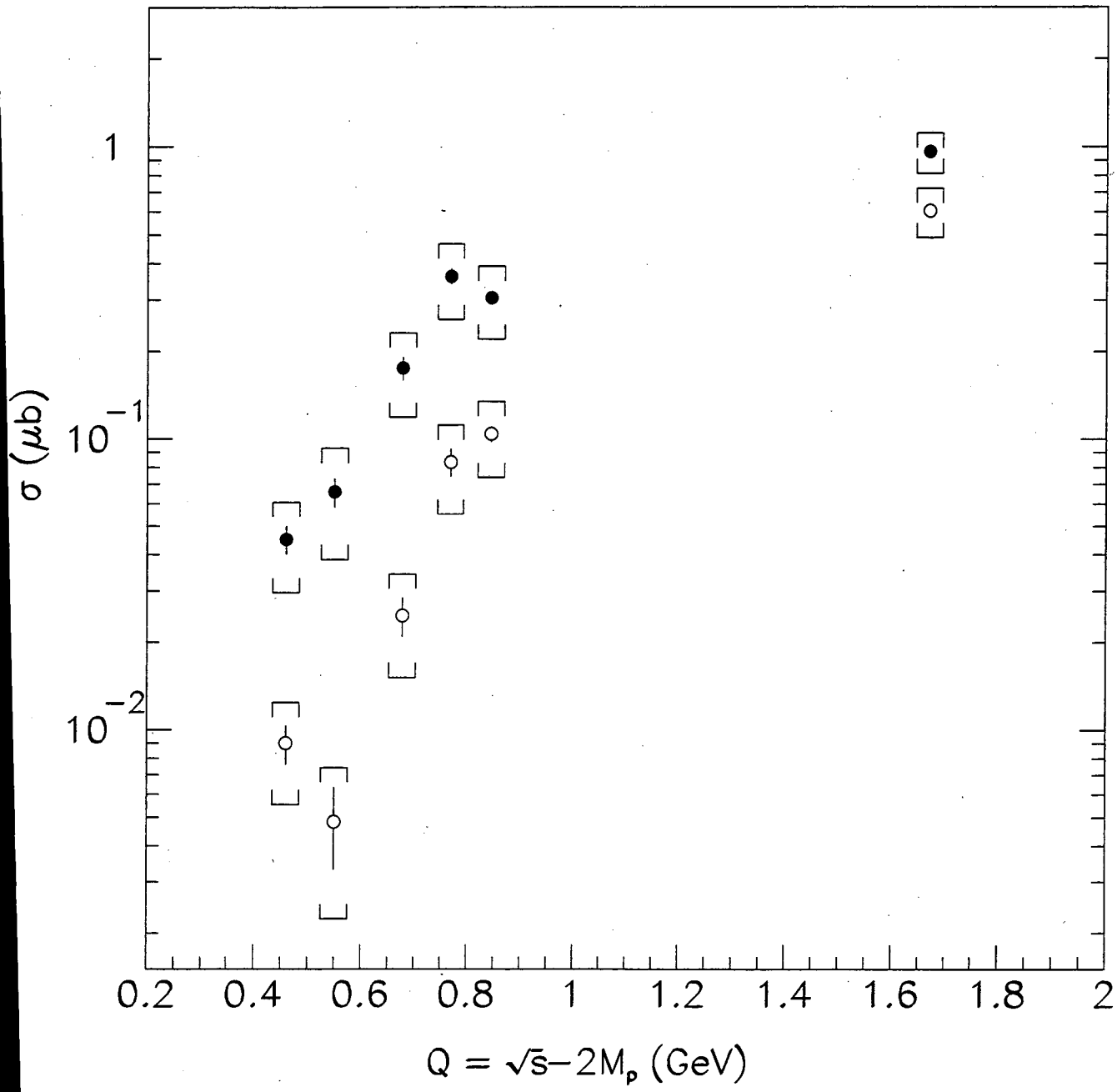

figure 15

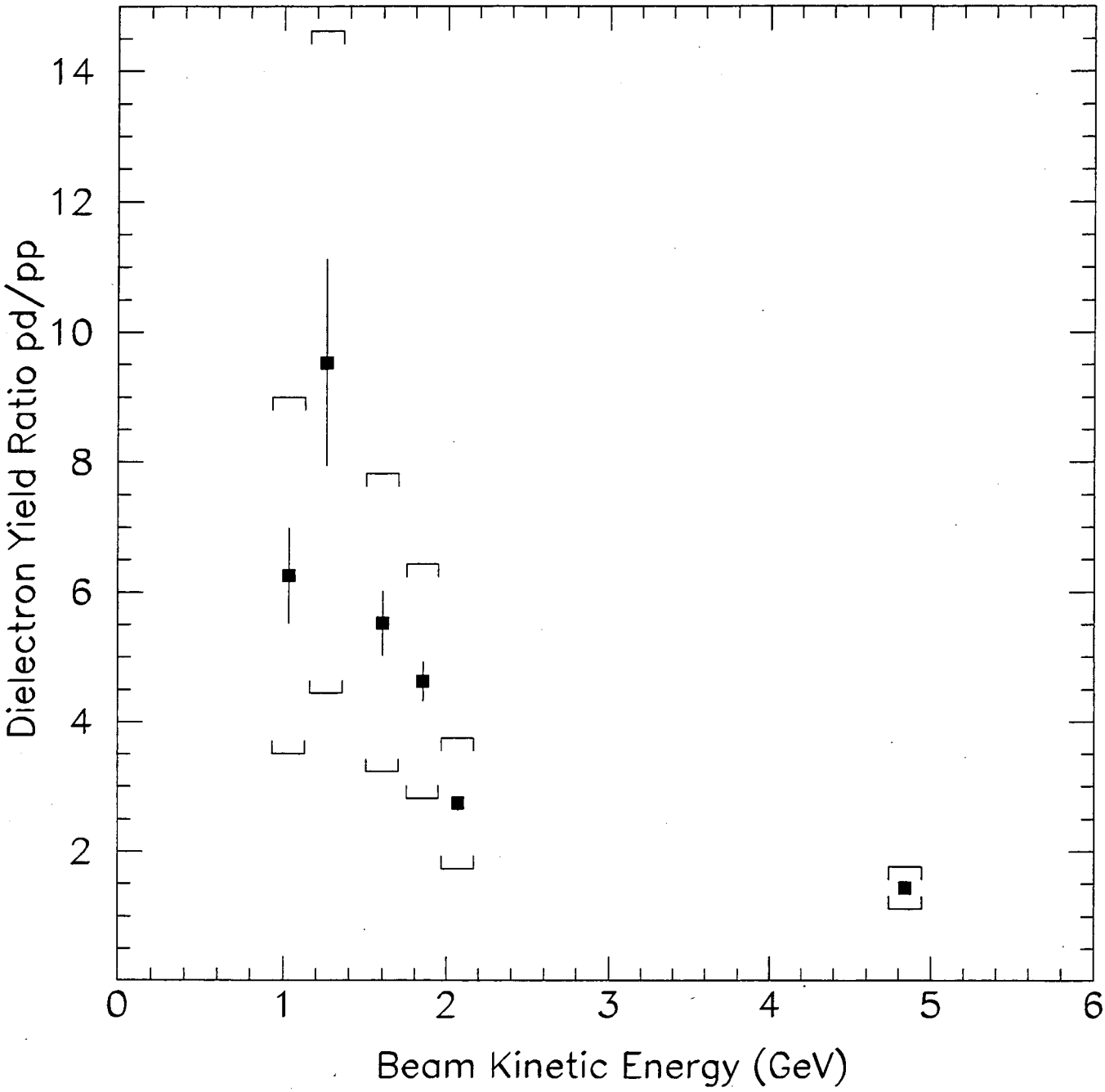
Dielectron Yield Ratio pd/pp
14
12
10
8
6
4
2
0
1
2
3
4
5
6
Beam Kinetic Energy (GeV)

figure 16

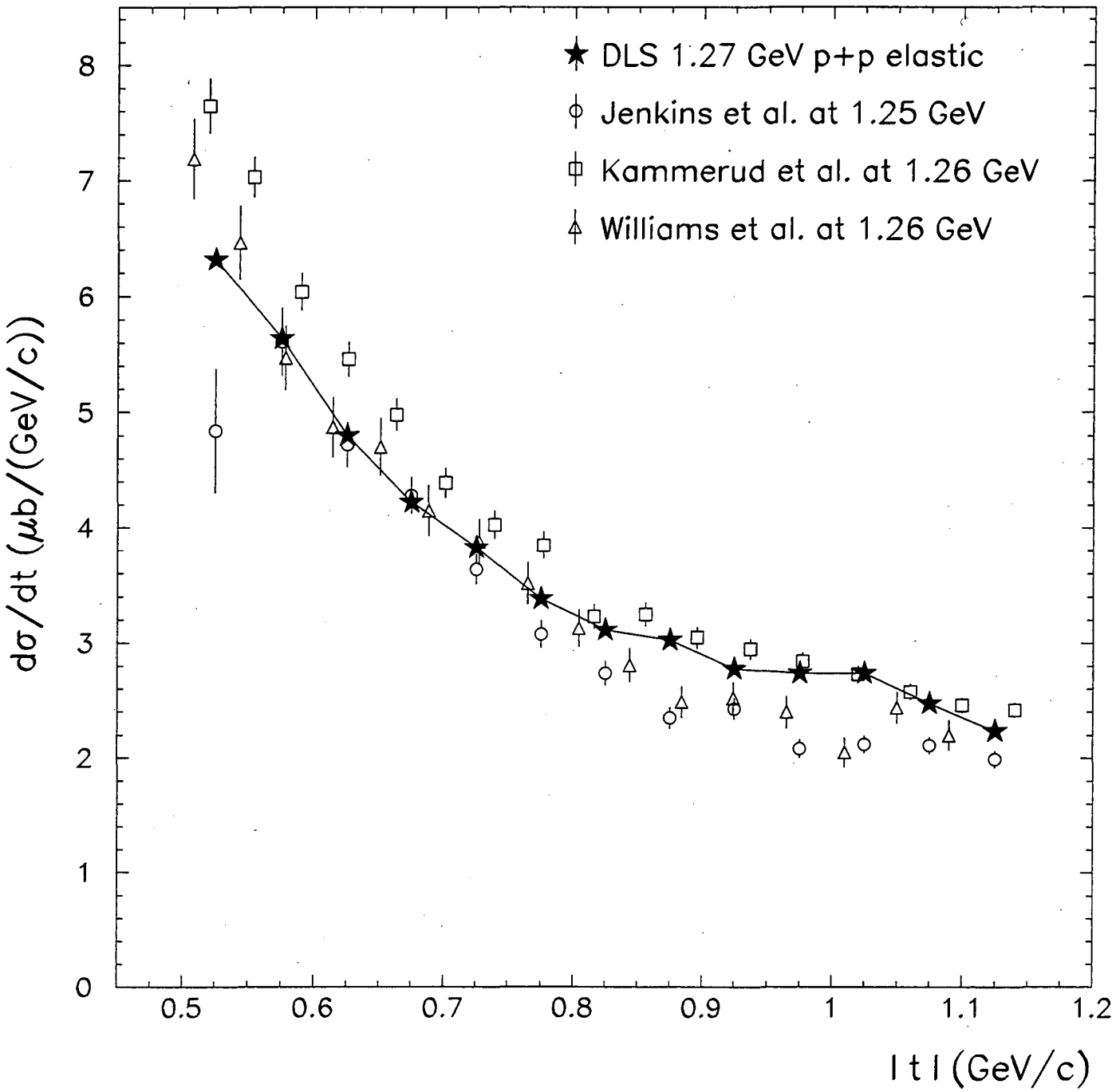
DLS 1.27 GeV p+p elastic
Jenkins et al. at 1.25 GeV
Kammerud et al. at 1.26 GeV
Williams et al. at 1.26 GeV
dσ/dt (μb/(GeV/c))
| t | (GeV/c)
0
1
2
3
4
5
6
7
8
0.5
0.6
0.7
0.8
0.9
1
1.1
1.2

Ernest Orlando Lawrence Berkeley National Laboratory
One Cyclotron Road | Berkeley, California 94720

Prepared for the U.S. Department of Energy under Contract No. DE-AC03-76SF00098